

TOBB UNIVERSITY OF ECONOMICS AND TECHNOLOGY
THE GRADUATE SCHOOL OF NATURAL AND APPLIED SCIENCES

**THE USE OF ANODIC ALUMINUM OXIDE MEMBRANES AS A SENSING
PLATFORM FOR SURFACE-ENHANCED RAMAN SPECTROSCOPY**

MASTER THESIS
Merve ÇELİK

Department of Biomedical Engineering

Supervisor: Assoc. Prof. Dr. Fatih BÜYÜKSERİN

DECEMBER 2017

Approval of the Graduate School of Natural and Applied Sciences.

.....
Prof. Dr. Osman EROĞUL
Director

I certify that this thesis satisfies all the requirements as a thesis for the degree of Master of Science.

.....
Prof. Dr. Osman EROĞUL
Head of Department

This is to certify that I have read this thesis, “**THE USE OF ANODIC ALUMINUM OXIDE MEMBRANES AS A SENSING PLATFORM FOR SURFACE-ENHANCED RAMAN SPECTROSCOPY**”, by **Merve Çelik** defended on 05.12.2017 and that in my opinion it is fully adequate, in scope and quality, as a thesis for the degree of Master of Science.

Supervisor: Assoc. Prof. Dr. Fatih BÜYÜKSERİN
TOBB University of Economics and Technology

Examining Committe Members :

Prof. Dr. Osman EROĞUL (President)
TOBB University of Economics and Technology

Assoc. Prof. Dr. Gökhan DEMİREL
Gazi University

TEZ BİLDİRİMİ

I hereby declare that all the information provided in this thesis was obtained with rules of ethical and academic conduct. I also declare that I have cited all sources used in this document, which is written according to the thesis format of the TOBB University of Economics and Technology Institute of Natural and Applied Sciences.

Tez içindeki bütün bilgilerin etik davranış ve akademik kurallar çerçevesinde elde edilerek sunulduğunu, alıntı yapılan kaynaklara eksiksiz atıf yapıldığını, referansların tam olarak belirtildiğini ve ayrıca bu tezin TOBB ETÜ Fen Bilimleri Enstitüsü tez yazım kurallarına uygun olarak hazırlandığını bildiririm.

Merve Çelik

.....

ABSTRACT

Master of Science

THE USE OF ANODIC ALUMINUM OXIDE MEMBRANES AS A SENSING PLATFORM FOR SURFACE-ENHANCED RAMAN SCATTERING

Merve ÇELİK

TOBB University of Economics and Technology
Institute of Natural and Applied Sciences
Biomedical Engineering

Supervisor: Assoc. Prof. Dr. Fatih BÜYÜKSERİN

Date: December 2017

Despite the potential sensitivity and the wide range of applications for Surface Enhanced Raman Spectroscopy (SERS), it can not be used as a routine diagnostic tool due mainly to the poor reproducibility of the high intensity SERS signals. In order to obtain reproducibly strong SERS signals, both lithographic and non-lithographic approaches are intensively investigated to produce large-area nanopatterned SERS substrates displaying periodically decorated arrays of nanostructures. Herein, two non-lithographic methods for fabricating periodically decorated plasmonic nanoparticle arrays by using anodic aluminum oxide membranes are presented. These membranes are a class of special biomaterials that are produced from high purity aluminum via two step anodization protocol. The production of these substrates are easy and highly controllable and compared to lithography it is cost-effective.

The first part of the study proposes the use of nanobump-decorated barrier sides of the anodic aluminum oxide membranes (AAMs) as SERS substrates. In order to investigate the effect of surface topography on SERS signal intensities, the nanobump-decorated surface (NBDS) is further treated with wet etching to create periodic arrays of nanocraters. SEM and AFM characterizations are performed for

the produced platforms. After coating with an optimized thickness of Au through PVD, SERS signal intensities of the nanocrater decorated surfaces (NCDS) and NBDS counterparts are compared by using two different model dyes, Methylene Blue and Congo Red. The experimental data is then confirmed with computer simulations using Comsol 5.0 Optics Module and Lumerical FDTD Solutions. Reproducibility of the signals and the lowest detectable concentration are also investigated.

In the second part of the study, the effect of the AAMs pore-size is examined, as they are used as molds to obtain periodically nanopillar-decorated polycarbonate surfaces. Two different pore-sized AAMs are used and silver reduction is performed by coating the surfaces with polydopamine, for the facile creation of plasmonic effect. The obtained surfaces are characterized by SEM and AFM. The intensities of the SERS signals from the obtained surfaces are compared by using Methylene Blue and also is verified with computer simulations using Lumerical FDTD Solutions.

Keywords: SERS, AAMs, Periodicity, Reproducibility, Sensing.

ÖZET

Yüksek Lisans Tezi

ANODİK ALUMİNYUM OKSİT MEMBRANLARIN YÜZEY-ARTTIRILMIŞ
RAMAN SPEKTROPİSİ İÇİN SENSÖR PLATFORMU OLARAK KULLANIMI

Merve ÇELİK

TOBB Ekonomi ve Teknoloji Üniversitesi
Fen Bilimleri Enstitüsü
Biyomedikal Mühendisliği Anabilim Dalı

Danışman: Doç. Dr. Fatih BÜYÜKSERİN

Tarih: Aralık 2017

Yüzey-arttırılmış Raman Spektroskopisi (SERS); geniş kullanım alanına sahip olması ve hassasiyetine rağmen sinyal tekrarlanabilirliği sorunlarından dolayı rutin tespit yöntemi olarak kullanılamamaktadır. Yüzey-arttırılmış Raman sinyallerini tekrarlanabilir ve yüksek şiddette elde edebilmek için litografik ve litografik olmayan bir çok yöntem kullanılarak geniş alanlı periyodik nanodekorasyonlu platformlar üretilmiştir. Bu çalışmada, litografik olmayan bir yöntem olarak yüksek saflıktaki alüminyumun iki-aşamalı anodizasyonu ile elde edilen anodik alüminyum oksit membranlar (AAM) kullanılarak iki farklı strateji ile farklı topografilerde yüzeyler elde edilmiştir. Önerilen sistemlerle yüzeylerin üretimi parametrelerle kontrol edilebilir ve kolaydır, litografik yöntemlere göre de ucuzdur.

Tezin ilk kısmında AAM'lerin nanotümsek dekorasyonlu bariyer yüzünün SERS yüzeyi olarak kullanımı araştırılmıştır. Yüzey topografisinin SERS sinyal şiddeti üzerine etkisini incelemek için, nanotümsek dekorasyonlu yüzeyler (NTDY) asitle aşındırılarak periyodik nanokrater dekorasyonlu yüzeyler (NKDY) elde edilmiştir.

Üretilen yüzey karakterizasyonları TEM ve AKM ile yapılmıştır. Fiziksel buharla kaplama yöntemiyle optimum altın kalınlığıyla kaplanan yüzeylerden alınan SERS sinyal yoğunlukları, Metilen Mavisi ve Kongo Kırmızı model boyaları kullanılarak

karşılaştırılmıştır ve alınan deneysel sonuçlar Comsol 5.0 Optik Modülü ve Lumerical FDTD Solutions simülasyon programları kullanılarak da desteklenmiştir. Sinyal tekrarlanabilirliği ve tespit edilebilir en düşük metilen mavisi konsantrasyonu da araştırılmıştır.

Tezin ikinci kısmında farklı por çapına sahip AAM'ler kalıp olarak kullanılarak periyodik nanosütun dekorasyonlu polikarbonat yüzeyler üretilmiştir. Üretilen iki farklı nanosütun çapına sahip yüzeyler pratik ve ucuz bir yöntem olarak üzerlerine polidopamin kaplama sonrası gümüş nanoparçacıklar çöktürülerek plazmonik etki yaratılmıştır. Üretilen yüzeyler TEM ve AKM ile karakterize edilmiştir. Üretilen farklı yüzeylerden elde edilen Metilen Mavisi sinyalleri karşılaştırılmış ve alınan sinyaller Lumerical FDTD Solutions simülasyon programı kullanılarak desteklenmiştir.

Anahtar Kelimeler: SERS, AAMs, Periyodiklik, Tekrarlanabilirlik, Algılama.

ACKNOWLEDGEMENT

I would like to thank:

My supervisor Assoc. Prof. Dr. Fatih Büyükserin for his guidance, patience and wisdom during my entire Master Degree and for giving me a chance to work with him,

Assoc. Prof. Dr. Gökhan Demirel who always supports and enlightens me generously,

Prof. Dr. Uğur Tamer for making it possible to carry out our Raman measurements in his laboratory and Prof. Dr. Hamza Kurt for using his laboratory for computer simulations,

Büyükserin Research Group members, who were always there for me when I was in need,

TOBB University of Economics and Technology for financially supporting me with a scholarship during my Master Degree,

My dearest friends Burçe, Irmak Ö., Emre, Ozan, Koray, Irmak E. who bear with me through this process and be there for me all the time,

My mother for her eternal love and support and making me realise how lucky I am through my ups and downs, my father whose efforts and care made me who I am today and Metehan for being my little beloved brother,

This thesis is dedicated to my precious family and my great nation.

TABLE OF CONTENTS

	<u>Page</u>
ABSTRACT	iv
ÖZET	vi
ACKNOWLEDGEMENT	viii
TABLE OF CONTENTS	ixx
LIST OF TABLES	xi
LIST OF FIGURES	xii
LIST OF ABBREVIATIONS	xiv
1. INTRODUCTION	1
1.1 Introduction	1
1.1.1 Anodic aluminum oxide membranes (AAMs).....	2
1.1.2 Raman spectroscopy	6
1.1.3 Surface-enhanced Raman spectroscopy (SERS)	7
1.1.4 SERS platforms.....	8
1.1.5 Anodic aluminum oxide membranes as SERS platforms	10
1.1.6 Aim.....	10
2.BARRIER SIDE OF ALUMINUM OXIDE MEMBRANES AS SERS PLATFORMS	13
2.1 Introduction	13
2.1.1 Barrier side of AAMs	13
2.1.2 Modification of the topography for improving SERS signals	15
2.1.3 Aim	15
2.2 Experimental	16
2.2.1 Materials	16
2.2.2 Methods	16
2.2.2.1 Fabrication of AAMs	16
2.2.2.2 Fabrication of NBDS and NCDS substrates	16
2.2.2.3 Characterization of the produced platforms.....	18
2.2.2.4 SERS sample preparation and SERS measurements	18
2.2.2.5 Computational simulations	18
2.2.2.6 Enhancement factor calculation.....	19
2.3 Results and Discussion.....	19
3. ANODIC ALUMINUM OXIDE MEMBRANES AS A MOLD FOR FABRICATING POLYMER-BASED SERS SUBSTRATES WITH TUNABLE PROPERTIES	33
3.1 Introduction	33
3.1.1 Adjusting the mold topography	34
3.1.2 Aim	34
3.2 Experimental	35
3.2.1 Materials	35
3.2.2 Methods	35
3.2.2.1 Fabrication of AAMs	35
3.2.2.2 Hydrophobic coating on AAMs.....	35

3.2.2.3 Fabrication of nanopatterned PC films.....	36
3.2.2.4 Dopamine coating to PC films and silver deposition.....	37
3.2.2.5 Characterization of the produced platforms.....	37
3.2.2.6 SERS sample preparation and SERS measurements.....	37
3.2.2.7 Computational simulations.....	37
3.3 Results and Discussion.....	38
4. CONCLUSION	47
5. FUTURE WORKS.....	49
REFERENCES.....	51
BIOGRAPHICAL SKETCH.....	57



LIST OF TABLES

	<u>Page</u>
Table 2.1 : Experimental and literature values for some of signature Raman shifts of MB and CR dyes.....	25
Table 2.2 : RSD values for the Raman shifts of MB collected from Au@NCDS substrates.....	29
Table 3.1 : RSD values for the Raman shifts of MB collected from Aq@LNPC substrates.....	43

LIST OF FIGURES

	<u>Page</u>
Figure 1.1 : Schematic of the two-step anodization process.....	3
Figure 1.2 : SEM micrographs of (a) solution side, (b) barrier side, (c) cross-section of anodic aluminum oxide membranes.....	4
Figure 1.3 : Schematic representation of the fields that AAMs used.....	5
Figure 1.4 : Schematic of energy changes after light-molecule interaction.....	6
Figure 2.1 : SEM micrographs of (a) porous side and (b) barrier layer and (c) schematic depiction of AAMs morphology.....	14
Figure 2.2 : Schematic representation of the NBDS and NCDS substrate fabrication. Normally AAM films form on both sides of the Al foil, but only one side of the AAM film was represented for simplicity.....	17
Figure 2.3 : (a) Photograph and (b) SEM micrographs of NBDS substrates. After a 90 min. acid treatment, (c) NCDS substrates displaying nanocratered topography can be obtained. The inset figures are higher magnification SEM images displaying the hexagonal packing of the nanopatterns.....	19
Figure 2.4 : SEM images of NBDS substrates treated with (a) 5% wt. phosphoric acid for 30 minutes, (b) 5% wt. phosphoric acid for 90 minutes, (c) 5% wt. phosphoric acid for 30 minutes followed by 30 minutes of 5% wt. sulfuric acid treatment, electropolish solution for (a) 30, (e) 90 and (f) 120 minutes.....	21
Figure 2.5 : Calculated diameter frequency distributions of (a) nanobumps of NBDS and (b) nanocrater gaps of NCDS.....	22
Figure 2.6 : AFM images of (a) 20nm-Au@NBDS and (b) 20nm-Au@NCDS substrates.....	23
Figure 2.7 : SERS signals of 10^{-3} M MB obtained from 10, 20 or 30 nm thick Au- coated (a) NBDS and (b) NCDS substrates.....	24
Figure 2.8 : (a) MB and (b) CR SERS signals obtained from NCDS, NBDS and flat alumina substrates after 20 nm Au coating.....	27

Figure 2.9 : Simulated electric field around the constituent individual (a) Au sphere, (b) torus representing Au@NBDS and Au@NCDS substrates respectively.....	28
Figure 2.10 : SERS spectra of MB collected from 30 random spots of 3 independent Au@NCDS substrates.....	29
Figure 2.11 : (a) SERS spectra of MB with different concentrations and (b) logarithm of MB concentration against the corresponding intensities at the 1621 cm^{-1} peak for Au@NCDS substrates. Blue line in (b) represents the linear region.....	31
Figure 2.12 : SERS spectra of 10^{-3} M MB on Au@NCDS for different resting periods.....	32
Figure 3.1 : Schematic representation of the fabrication of nanopatterned PC films by using hydrophobically-modified AAM molds.....	36
Figure 3.2 : Photograph from contact angle measurement of AAM after ODTS coating.....	38
Figure 3.3 : SEM micrograph of (a) SNPC and (b) LNPC substrates.....	39
Figure 3.4 : Calculated diameter frequency distribution of (a) SNPC and (b) LNPC Substrates.....	39
Figure 3.5 : SEM micrographs of polydopamine coated (a) SNPC and (c) LNPC substrates and after 24 hours of silver deposition on (b) SNPC and (d) LNPC surfaces that have been polydopamine-coated.....	40
Figure 3.6 : MB SERS signals from Ag deposited SNPC (black) and LNPC (red) polycarbonate surfaces.....	42
Figure 3.7 : Simulated electric field around the constituent two adjacent Ag spheres with (a) 40,5 nm radius and (b) 53,5 nm radius representing Ag@SNPC and Ag@LNPC substrates respectively.....	43
Figure 3.8 : MB SERS spectra from LNPC substrates with different Ag deposition times.....	45

LIST OF ABBREVIATIONS

AAM	: Anodic Aluminum Oxide Membrane
AFM	: Atomic Force Microscopy
Ag@LNPC	: Silver deposited Large Nanopillar Polycarbonate
Ag@SNPC	: Silver deposited Small Nanopillar Polycarbonate
Au@NBDS	: Gold-coated Nanobump-decorated Surface
Au@NCDS	: Gold-coated Nanocrater-decorated Surface
CR	: Congo Red
EF	: Enhancement Factor
HOMO	: Highest Occupied Molecular Orbital
LNPC	: Large Nanopillar Polycarbonate
LOD	: Limit of Detection
LSP	: Localized Surface Plasmon
LUMO	: Lowest Unoccupied Molecular Orbital
MB	: Methylene Blue
NBDS	: Nanobump-decorated Surface
NCDS	: Nanocrater-decorated Surface
ODTS	: Octadecyltrimethoxysilane
PC	: Polycarbonate
PSP	: Propagating Surface Plasmon
RSD	: Relative Standard Deviation
SEM	: Scanning Electron Microscope
SERS	: Surface-enhanced Raman Spectroscopy
SNPC	: Small Nanopillar Polycarbonate
SPR	: Surface Plasmon Resonance

1. INTRODUCTION

1.1 Introduction

Nanotechnology is studying and working with one billionth of a meter, nanometer, sized object [1]. The National Nanotechnology Initiative of the United States describes nanotechnology as “the understanding and control of matter at the nanoscale, at dimensions between approximately 1 and 100 nanometers, where unique phenomena enable novel applications”. It comprises a variety of fields of science involving material, physics, medicine, engineering etc. While reducing the size from bulk to atomic or molecular state, the mechanical, optical, magnetic and electrical properties of the materials change, bringing both new challenges and opportunities for potential technologic approaches [2].

The new properties, which are size dependent in this nano-scale range, have led a potential technological progress in a variety of areas such as microelectronics, energy, cosmetics, nanomedicine and so on. Therefore, nanotechnology provides to create and manufacture functional materials, devices and systems by controlling materials in the nano-scale and using their novel phenomena and associated properties [3].

Nanomedicine, moreover, is the incorporation of medicine and nanotechnology and deals with the medical related, patient-centric nanotechnologies [4]. Nanosensors are a part of the research areas of nanomedicine. Concerns with the detection of trace levels of biological analytes lead to development in nanosensors.

Combining the unique properties of Raman spectroscopy and the advantages that nanotechnology offers, Surface-enhanced Raman Spectroscopy (SERS) was developed. Advances in the fabrication of nanomaterials also contribute to the development of SERS.

1.1.1 Anodic aluminum oxide membranes (AAMs)

Anodic aluminum oxide membranes (AAMs) are special class of biomaterials which are obtained by electrochemical oxidation of high purity aluminum [5]. In near-neutral electrolytes at ambient temperatures, contact films uniform in thickness are obtained. Moreover, in acidic electrolytes, regular porous anodic aluminum oxide films are formed [6]. Anodic aluminum oxide films with highly controllable morphologies can be achieved by selecting appropriate anodization conditions. AAMs are characterized by the following parameters: pore diameter, interpore distance, pore density, porosity, wall and barrier layer thicknesses. Depending on the applied potential, current, temperature and electrolyte type and concentration, the parameters can be tuned in the range of 10 to 400 nm for pore diameter, 50 to 600 nm for interpore distance, 10 nm to 150 μm for wall thickness, 10^9 to 10^{11} cm^{-2} for pore density and 5% to 50% for porosity [7-9].

In order to obtain highly controlled surface topography, AAMs are fabricated at certain conditions. By changing the parameters such as anodization voltage and time, electrolyte concentration and temperature; pore diameter, interpore spacing and film thickness could be adjusted [10]. Because there are many parameters to be optimized in electrochemical anodization process, the parameters that were optimized and standardized previously in our laboratory were used to obtain highly uniform periodic pore structure.

To obtain high uniformity in the surface topography, two-step anodization method that Masuda and Fukuda proposed is generally used [11]. In the two-step anodization technique, the first anodization is performed to achieve the order and the homogeneity of the pores on the surface. After dissolving the first layer with an acidic solution, pitches on the surface of the aluminum are obtained. With the second anodization at the same conditions as in the first one, regular pore formation occurs from the pitches and highly uniform and homogenous porous oxide layer is formed. (Figure 1.1)

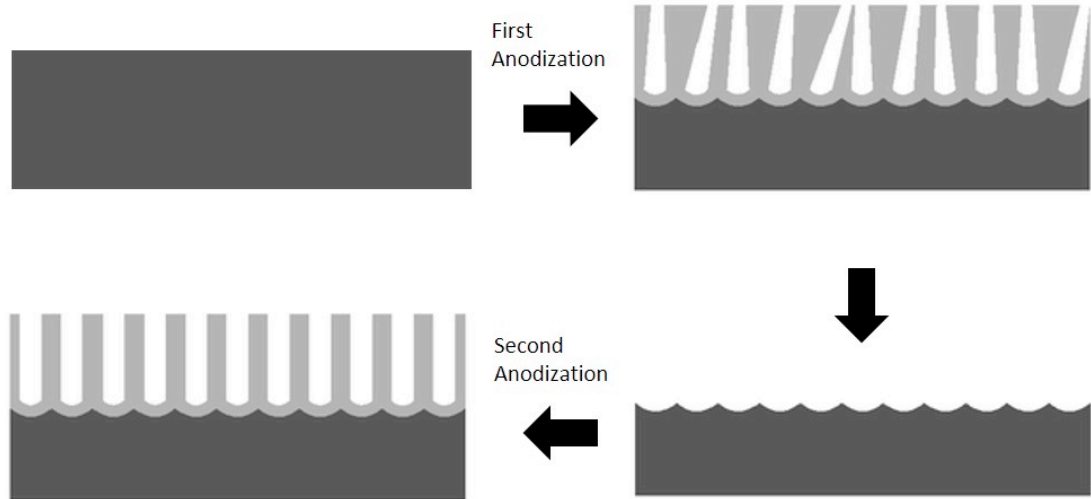


Figure 1.1 : Schematic of the two-step anodization process [12].

The solution and barrier sides and thickness of AAMs obtained from two-step anodization are shown in Figure 1.2. Regular and uniform pore formation on solution side (Figure 1.2 a) and bump formation on barrier side (Figure 1.2 b) could be achieved. On the other hand, commercial AAMs are available with 20, 100 and 200 nm pore size and 60 μm thickness [13]. The non-uniformity of the pore structures of these commercial surfaces however limits the nanotechnologic applications of them and the need for highly controllable lab-made AAMs arises.

The controllable physical and chemical properties of AAMs enables them to be used in a wide range of applications and can be categorized as biomedical, separation, sensing and electronics [14].

Chemical sensing and biosensing applications of AAMs gather great attention in recent years due to their unique properties. Compared to lithographic techniques which are time consuming and expensive, self-ordering electrochemical anodization offers various advantages including cost-effective fabrication of arrays of homogenous nanostructures that contribute to the sensing mechanism. By controlling the pore diameters, pore-to-pore distances, pore geometry and pore depth several different forms and arrangements of nanoparticle arrays are plausible via utilizing AAMs. The traditional use of AAMs as sensors can be classified on the basis of their optical and electrochemical-detection principles.

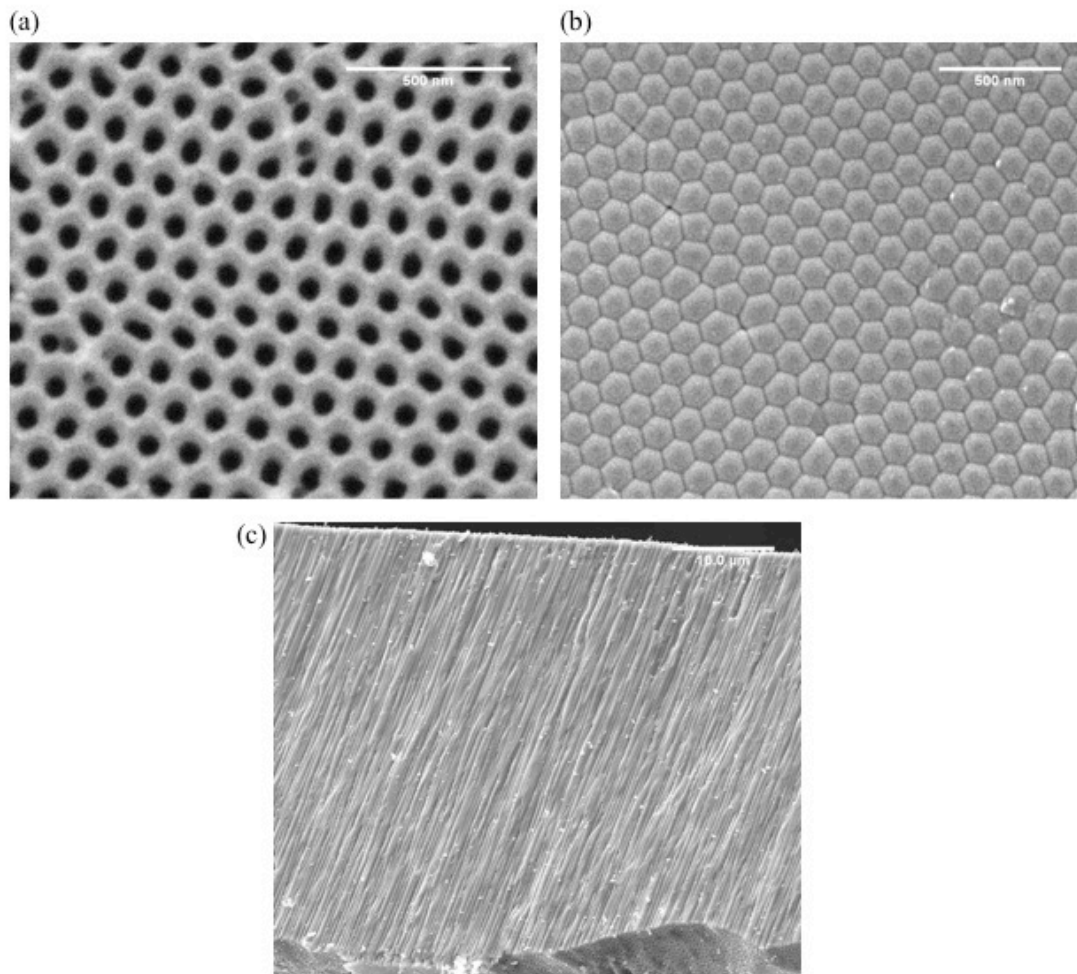


Figure 1.2 : SEM micrographs of (a) solution side, (b) barrier side, (c) cross-section of anodic aluminum oxide membranes.

Electrochemical sensors based on AAMs can be categorized as voltammetric, amperometric, conductometric, impedometric, capacitive and resistive. AAMs also show unique responses while interacting with light because of their geometry and chemical composition enabling them to be used as an optical sensing platform. AAMs have been shown to be used as a platform effectively especially for reflectance, absorbance, transmittance, photoluminescence, chemiluminescence and wave-guiding [15].

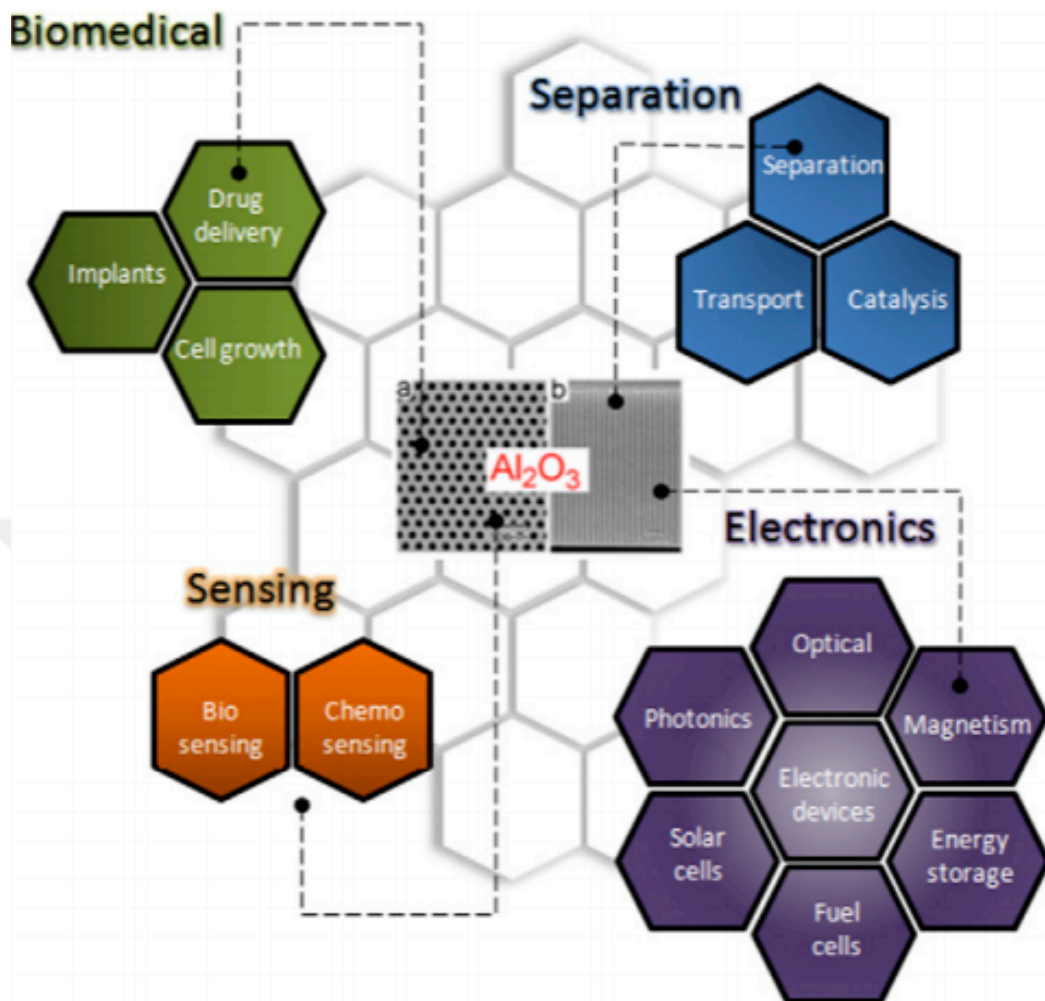


Figure 1.3 : Schematic representation of the fields that AAMs used.

1.1.2 Raman spectroscopy

Raman spectroscopy provides fingerprint information about the chemical structure of the molecules which enables label-free detection of the analyte by measuring the frequency shift of inelastic scattered light when the incident photon interacts with the sample [16-19]. The inelastic scattering causes an energy difference between the incident and scattered photons. The case where scattered photon has lower energy than the incident photon is called Stokes Raman scattering. If the scattered photon has higher energy than the incident photon, it is called anti-Stokes Raman scattering. In that case, the incident photon gets energy from the bond of the analyte molecule when the bond is already in the excited vibrational state. (Figure 1.4)

The shift in the incident photon's wavelength depends on the composition of analyte molecule and the magnitude of the change in the molecular polarization determines the intensity of Raman scattering. According to Raman selection rule, the change in the molecular polarizability is the result of the displacement of the constituent atoms from the equilibrium positions as the result of the molecular vibrations.

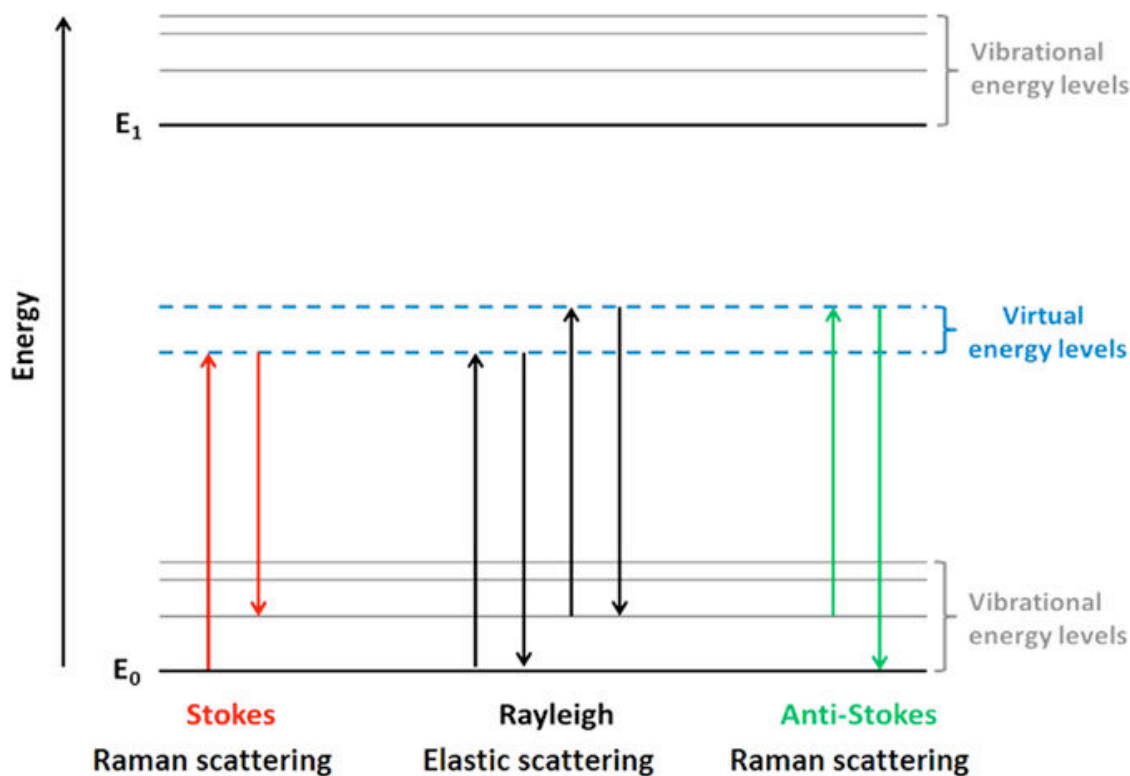


Figure 1.4 Schematic of energy changes after light-molecule interaction [20].

Raman spectroscopy has numerous advantages. The scattering of the incident light is measured so the bulk size and the bulk shape do not affect Raman spectroscopy. No sample preparation is needed and samples in solid, liquid or gaseous states can be analyzed. Raman spectroscopy is a non-destructive method and no vacuum is needed which simplifies this technique. The Raman spectrum is obtained relatively quickly and weak Raman scattering of water is also beneficial for analytes in aqueous solutions. The spectral bandwidths of Raman are much lower than those of other spectroscopic techniques such as Infra Red and Fluorescence, which makes this technique suitable for multiplex detection and identification of different chemicals in analyte.

Despite the advantages and potential of Raman spectroscopy, it also has several disadvantages. As the Raman cross-section is relatively low, Raman signal intensities

are low, which makes it hard to analyse samples with low concentration. The laser radiation is intense, so sample heating can be problematic. In certain cases, a large fluorescence background signal can be observed.

1.1.3 Surface-enhanced Raman spectroscopy (SERS)

Surface-enhanced Raman Spectroscopy (SERS) is an optical spectroscopic technique resulting in highly enhanced Raman signals of molecules on nanostructured conducting materials by taking advantage of surface plasmon resonances (SPR) [17, 21]. As a result of the surface enhancement, Raman cross-sections of molecules could be increased the details of which are explained below. The enhanced signals allow the detection of ultra-trace amounts of molecules down potentially to a single molecule level [19, 22].

Mechanisms of SERS

The enhancement of the Raman signals with SERS are attributed to two mechanisms. The first and the strongest mechanism is the electromagnetic enhancement which is related to the excitation of the surface plasmons with the incident light [23]. Interaction of the incident light with metallic nanoparticles induces polarization in the metallic nanoparticle. SPR can be obtained when an incoming electromagnetic radiation of certain frequency illuminates a nanostructure causing a collective oscillation of the structures' surface electrons. When this interaction occurs, the local electric field around metallic nanostructure will greatly increase, causing the effective increase in the absorbed as well as the scattered electromagnetic radiation from the plasmonic particle. Due to this enhanced scattering, the signature Raman peaks of analyte molecules in the close proximity of the metal nanoparticles can be increased up to 10^{14} folds compared to their regular Raman shifts [24].

Surface plasmons are categorized into two types: propagating surface plasmons (PSP) and localized surface plasmons (LSP). Whether a nanostructured surface shows LSP or PSP depends on the structure and dimension of the substrate [25].

PSPs are the electromagnetic waves propagating between metal/dielectric interface. Continuous metallic nanostructures enable stimulation of PSP. LSPs, on the other hand, are the electromagnetic waves formed in relatively small areas where surface

electrons are confined. LSP can be enhanced by highly rough nanometallic surfaces. The nanogaps at sharp tips or edges of metallic nanostructures when radiated with electromagnetic waves are called hotspots, resulting in highly enhanced localized electric fields. The presence and density of hotspots are mainly effective on the SERS signal enhancement [26]. Stimulating both localised and propagating surface plasmon resonances will result in further enhancement of produced electric field.

The second and the less effective mechanism is chemical enhancement which depends on the level of interaction between noble metal surface and analyte. Charge transfer between analyte and surface forms the basis of this chemical mechanism. Metallic nanostructures help the charge transfer between the analytes' highest occupied molecular orbital (HOMO) and lowest unoccupied molecular orbital (LUMO) although very recently organic semiconductors have been shown to facilitate this phenomenon as well [27]. The overall chemical enhancement depends on the chemical nature of the analyte and varies from molecule to molecule.

1.1.4 SERS platforms

Despite the high sensitivity and specificity of SERS, this technique can not be used as a routine detection tool because of the irreproducibility of the signals. SERS measurements from SERS substrates, which are generally metallic nanoparticles and nanostructured metal surfaces, and their reproducibility and SERS efficiencies determine its application. The ultimate goal is to achieve highly enhanced Raman signals of analytes in a reproducible manner [28].

As the potential of the SERS technique is explored, a wide range of SERS substrates have been developed and fabricated in the last few decades. The first SERS substrates used in history were roughened noble metal surfaces and noble metal colloids. Since then the strategies to fabricate SERS substrates can be divided broadly into three categories; chemical synthesis, template-assisted methods and lithographic patterning.

Metal suspensions or aggregates obtained by chemical synthesis have been used widely in SERS applications because of the ease of their preparation and adjustable parameters [29]. Enhancement factors up to 10^{14} have been reported, allowing detection down to a single molecule [24]. Despite the high signal enhancements that

metal colloids and aggregates offer, reproducibility of the obtained signals is a challenge. Further researches to achieve reproducibility have been done by positioning nanoparticles on a substrate with controlled localization of nanoparticles. Pre-determination of the locations enables hotspot engineering and reproducibility of the obtained SERS signals.

Developments in template-assisted fabrication lead a broad range of SERS substrates to be produced. The use of templates can control the surface structure, therefore tuning the plasmonic material's geometry as well as improving the reproducibility are plausible. Control over both the template and the metallic layer thickness enrich the utility and advantages of this approach.

Considerable amount of research is done to develop powerful plasmonic arrays for SERS applications due to the reproducibility of SERS signals with low spot-to-spot and sample-to-sample differences. The most common methods used for creating metallic nanostructure arrays are electron beam lithography, nanosphere lithography, focused ion beam patterning and soft-lithography. Optimal control over particle shape and arrangement is doable with such techniques, however, limitations like high-cost, difficulties in application especially for applying on large surfaces limits their extensive usage [30].

The criteria for a nanostructured metallic surface to be an ideal SERS substrate suitable for routine diagnostics can be stated as follows: The nanostructures should be arranged regularly or periodically for obtaining a collective electric field from adjacent structures also enabling low spot-to-spot Raman signal intensity differences. The signal intensities and enhancement have to be homogenous from spot-to-spot causing reproducibility of the obtained SERS signals, therefore, making this technique suitable for routine diagnostic applications. The surface should be stable for long-time and insensitive to the environmental factors. Moreover, the surface has to be biocompatible for biologic applications. The surface should provide large signal enhancements enabling detection of low concentrated and small amount of analytes. The fabrication procedure of the substrates should be reproducible, cost-effective and easy [24].

1.1.5 Anodic aluminum oxide membranes as SERS platforms

Self-ordered and self-assembled fabrication processes are known as cost effective and elegant techniques for obtaining complex and functional nanostructured materials [31, 32]. AAMs, due to their unique properties such as chemical, thermal stability, hardness and high surface area, stand out from other techniques.

Nanoporous anodic aluminum oxide membranes are unique materials that can possess hexagonally arranged arrays of nanopores through anodizing high purity aluminum metal [5]. Moreover, pore diameter, pore-to-pore distance and overall porosity of these ceramic membranes can be easily tuned by optimizing process parameters like voltage, electrolyte and pre-patterning conditions [33]. Stemming from this ability, both the electrolyte-interfacing solution side [34, 35] and the metal-interfacing barrier side of AAMs [36, 37] were received attention and studied for developing large area nanopatterned SERS substrates after a thin metal coating step. AAM-driven SERS substrates are fabricated commonly by evaporating or sputtering metallic layer of gold or silver on the solution or barrier side of the porous material. By tuning the metal coating conditions, homogenous arrays of plasmonic nanostructures with various geometries can be obtained [15].

1.1.6 Aim

As stated in the previous sections, although SERS is a highly sensitive and a specific technique, it can not be used as a routine detection tool because of its reproducibility problems. Significant spot-to-spot and substrate-to-substrate signal variations are observed especially when traditional colloidal nanoparticle-driven SERS substrates are employed. In order to obtain reproducibly strong SERS data, both lithographic and non-lithographic approaches are intensively investigated to produce large-area nanopatterned SERS substrates displaying periodically arranged arrays of nanostructures. AAMs display highly ordered and controllable nanocolumned structures which can be used as SERS substrates in various ways. This non-lithographically fabricated material could be utilized for the preparation of SERS substrates for routine diagnostic applications, due to its facile and reproducibly fabricated homogenous morphological nature and robust material characteristics.

Herein, AAMs were employed in two different approaches for the non-litographic fabrication of robust SERS substrates displaying plasmonic nanoparticle arrays for routine diagnostic analysis for SERS.





2. BARRIER SIDE OF ANODIC ALUMINUM OXIDE MEMBRANES AS SERS PLATFORMS

2.1 Introduction

2.1.1 Barrier side of AAMs

In the literature, the most common methods used for creating metallic nanostructured arrays are electron beam lithography, nanosphere lithography, focused ion beam patterning and soft-lithography which have limitations like high-cost, difficulties in application especially for applying on large surfaces [38]. It is also stated that periodically nano-decorated arrays significantly contribute to high signal enhancements due to the hotspot and collective electric field generation. In the rational design of the SERS substrates, closer the nano structures get, higher the signal enhancement is. Moreover, it was indicated that structures that touch and interact strongly causes very localized plasmon modes which yields high signal enhancement.

AAMs are used for more than hundred years for mainly filtering applications. Commonly used electrolytes in the fabrication of AAMs are sulfuric, oxalic and phosphoric acids [39]. The self-organized pore structures are obtained by anodization of aluminum at certain conditions. The solution side (Figure 2.1.a) is the face of the ceramic material that faces the electrolyte. It displays a porous morphology and the pore size, porosity and inter-pore distance parameters can be controlled by electrolyte type and concentration and voltage [40]. At the bottom of every pore structure, a U-shaped homogenous barrier oxide layer (Figure 2.1.b) with 20-30 nm thickness is formed. This is the non-porous side which has bump-like topography, that faced the aluminum metal [41]. This face however can be exposed by removing the aluminum metal [42], and also the nanobumps can be etched to obtain membranes with open pores on both the solution and the barrier sides.

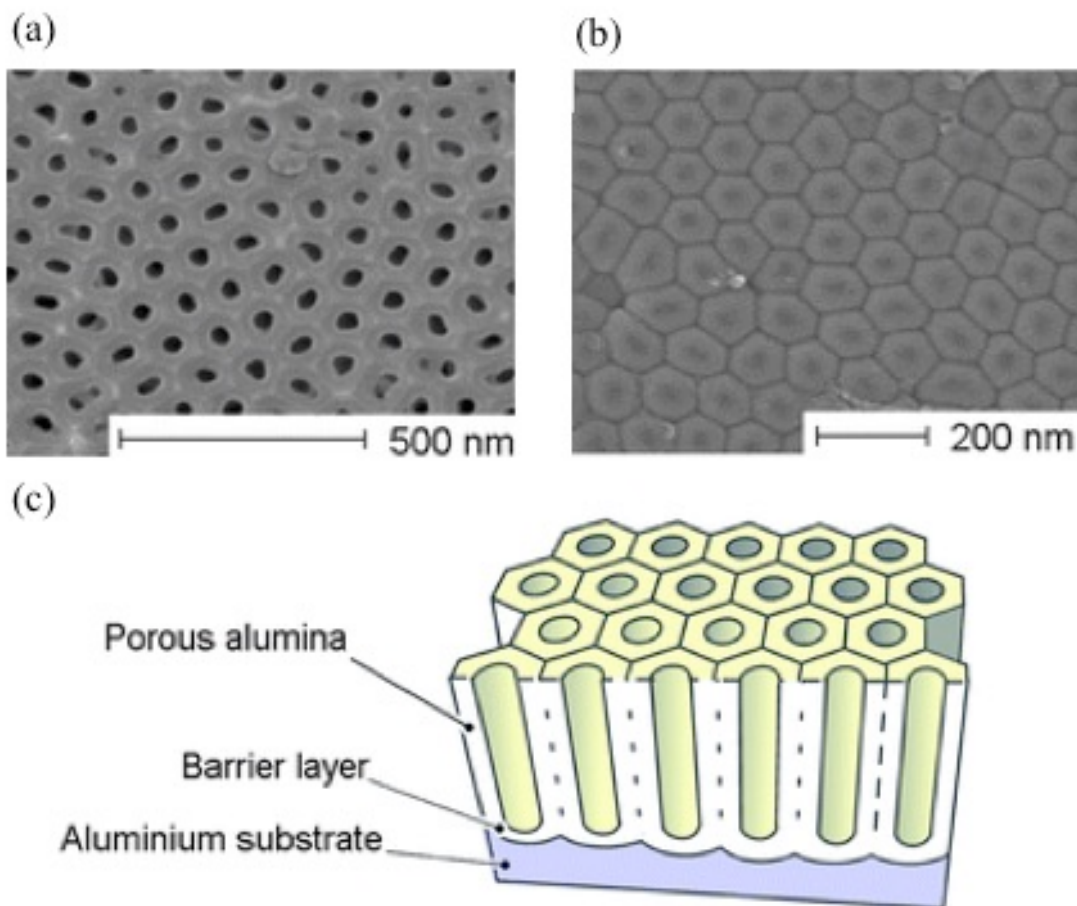


Figure 2.1 SEM-micrographs of (a) porous side and (b) barrier layer and (c) schematic depiction of AAMs morphology [43].

In terms of AAM use for SERS applications, both the solution as well as the barrier sides of these ceramic membranes were investigated as large area nanopatterned SERS substrates. Of particular interest, regular [44] or hierarchical [45] nanobump superlattice arrays were formed upon Ag evaporation onto the AAM barrier sides displaying nanobump-decorated surfaces. Although the long term stability of silver and the use of sophisticated e-beam or magnetron based evaporation methods can be criticized, these reports successfully demonstrated the modulation of SERS signals by varying the anodization and metal coating conditions, which alters the hotspot densities on the substrate surface.

The use of Au plasmonic particles on the other hand is preferred in many SERS applications, due mainly to increased signal and substrate stabilities compared to Ag and Cu nanoparticles [46].

2.1.2 Modification of the topography for improving SERS signals

It has been reported that the geometry and the arrangement of plasmonic nanoparticles have direct influence on SERS signals. For instance, the sharper the edges of these closely ordered structures, the higher the electromagnetic enhancement is. Roughness values in the 10-100 nm range contributes 10^4 to the overall signal enhancement [47]. Thus higher Raman signal enhancements will be achieved with sharper curvatures in the structure. Also metallic nanostructures' arrangement can provide cavity resonances. Therefore, intense hot spot generation occurs, resulting in highly enhanced signals. Another strategy that would increase the electromagnetic enhancement is to excite both propagating and localized surface plasmon by obtaining a continuous metallic coating on rough and curved nanostructured surfaces causing further signal enhancement.

2.1.3 Aim

We have previously developed an easy approach for obtaining free standing AAMs displaying porous solution sides and nanobump decorated barrier sides [42]. The barrier side of AAMs offers a large-area nanopatterned substrates with periodically arranged arrays of nanobumps with a non-litographic method. Our aim in this study was to first demonstrate that nanobump-decorated AAMs can be used as reproducible and robust SERS platforms due to the stable nature of the ceramic material as well as ordered arrays of nanobumps that becomes patterned plasmonic particles upon an optimum thickness of Au evaporation. Furthermore, in order to examine the influence of changing surface topography on SERS signals, the nanobumps were converted to nanocraters via wet-etching. As a result, substrates with nanocrater-decorated surfaces (Au@NCDS) showed improved signal intensities for two different model dyes when compared to Au-coated nanobump-decorated surfaces (Au@NBDS). The details of these findings are discussed below.

2.2 Experimental

2.2.1 Materials

High purity Aluminum foils (99.999%, Puratonic, 1 mm thickness), Congo Red (CR) and Methylene Blue (MB) were purchased from Alfa Easer. Acetone, HCl, H₂SO₄, NaOH, H₃PO₄ and C₂H₂O₄ were obtained from Sigma Aldrich. CrO₃ was purchased from Prolabo and Silicon <100> wafers were obtained from MicroChemicals GmbH. Deionized (DI) water (18 MΩ) was obtained from a Thermo Scientific Smart2pure system.

2.2.2 Methods

2.2.2.1 Fabrication of AAMs

Nanoporous AAMs were prepared by two-step anodization method [11]. High purity aluminum foil (99.999%) was sanded with 600 grit sand paper and sonicated in water. Further sonication with acetone was performed in order to get rid off the organic residuals. The foil was then electrochemically polished using a Pb cathode in an acidic solution (95% H₃PO₄, 5 wt% H₂SO₄ and 20 g/mL CrO₃) under 15 V at 65 °C for 90 minutes. Electropolished foils were anodized using 0.3 M oxalic acid as electrolyte against stainless steel at 5 °C under 50 V for 15 hours in the first anodization. The non-uniform alumina (Al₂O₃) layer formed on the both side of Al foil was then removed using 0.4 M H₃PO₄ and 0.2 M CrO₃ solution at 75 °C. A second anodization step was then applied at the same conditions as in the first one to obtain AAM films with periodically ordered hexagonal nanopores on both sides of the aluminum foil.

2.2.2.2 Fabrication of NBDS and NCDS substrates

In order to obtain NBDS substrate, a technique proposed earlier was used [48]. One of the AAM films on the aluminum layer was covered with a protective polymer layer. The unprotected AAM film was removed by 1 M NaOH solution and the aluminum layer was removed by 0.1 M CuCl₂·2H₂O and 6.1 M HCl solution to yield free-standing NBDS substrate.

To create nanocratered surface topography, the NBDS film was treated with a solution containing 95 wt% H_3PO_4 , 5 wt% H_2SO_4 and 20 g/ml CrO_3 for 90 min. (Figure 2.2)

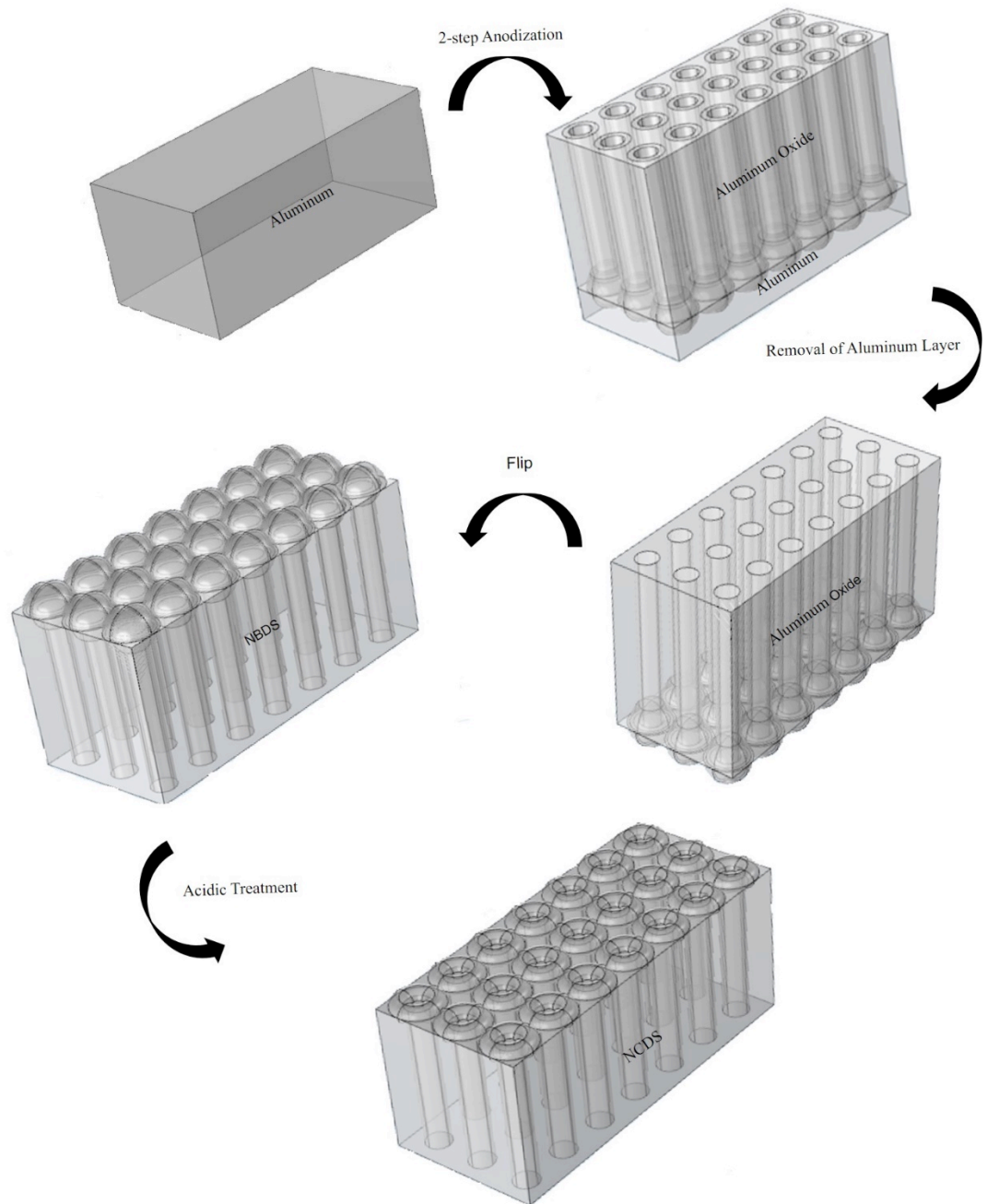


Figure 2.2 : Schematic representation of the NBDS and NCDS substrate fabrication. Normally AAM films form on both sides of the Al foil, but only one of the AAM films was represented for simplicity.

For control substrates in SERS measurements, flat 50 nm-thick non-porous alumina films were deposited on silicon <100> wafers via atomic layer deposition (Fiji F200-LL ALD reactor, Cambridge Nanotech Inc.).

In order to obtain SERS signals from these produced surfaces, gold coating was performed with a physical vapour deposition system (Nanovak HD) which works with a coating speed of 0.1 kÅ/sec under 10^{-5} torr.

2.2.2.3 Characterization of the produced platforms

Morphological characterization of the substrates were conducted by environmental scanning electron microscopy (SEM) (ESEM, FEI, Quante 200, 15 kV accelerating voltage) and atomic force microscopy (AFM) (ez-AFM, NanoMagnetics Instruments). PPP and SSS type cantilevers (Nanoworld AG) working at tapping mode were utilized for AFM measurements of the NBDS and NCDS substrates, respectively.

2.2.2.4 SERS sample preparation and SERS measurements

MB and CR were used as Raman reporters to evaluate the SERS performances of the fabricated surfaces as these two dyes were commonly used Raman-active dyes in the literature [49, 50]. 3 μ L aqueous solution of the Raman reporter was dropped on a \sim 1 cm x 1 cm gold-coated surface and the surface was kept in dark at room temperature until the Raman reporter dried. SERS measurements were collected with a Raman system (DeltaNu Examiner Laramie, WY, USA) using a cooled charge-coupled detector (CCD) in the range of 200-2000 cm^{-1} with 785 nm laser source. The measurements were done with 20 x objective, 3 μ m laser spot size, 60 s acquisition time and 150 mW laser power.

2.2.2.5 Computational simulations

In order to determine the formation of hotspots and demonstrate the electric fields around the Au-coated nanobumps, nanocraters, NBDS and NCDS, computer simulations were performed by Comsol 5.0 Optics Module. After investigation of the SEM and AFM images of the nanostructures and surfaces were modeled in this software. Using finite element method, electric field generations on the surfaces under 785 nm irradiation were simulated.

2.2.2.6 Enhancement factor calculations

Enhancement factor (EF) values are quantitative representations of the efficiencies for the different SERS substrates investigated. In this part of the study, 3 μL of aqueous MB solution was dropped on a 1 cm x 1 cm Au-coated substrate, and after the samples were dried, SERS spectra were acquired. EF was calculated by the following equation, where I_{SERS} and I_{Raman} are the intensities of MB at 1621 cm^{-1} obtained from Au-coated nanostructured and flat alumina surfaces, respectively [51]. Similarly, C_{Raman} and C_{SERS} are the concentrations of MB on Au-evaporated flat and nanostructured surfaces, respectively. Insertion of the employed concentrations and the corresponding extracted signal intensities into the below equation yields the total enhancement of the NBDS or NCDS substrates compared to flat alumina surface.

$$\text{EF} = (I_{\text{SERS}}/I_{\text{Raman}})(C_{\text{Raman}}/C_{\text{SERS}})$$

2.3 Results and Discussion

In the first part, studies for obtaining the desired topographies were carried out. After protecting one side of the AAM and dissolving the alumina and aluminum layers, a large area ($\sim 50\text{ cm}^2$) free-standing NBDS substrate was obtained (Figure 2.3.a). Morphological characterization of this material, i.e. the barrier side of the AAM films, reveals the formation of periodic arrays of nanobumps (Figure 2.2.b).

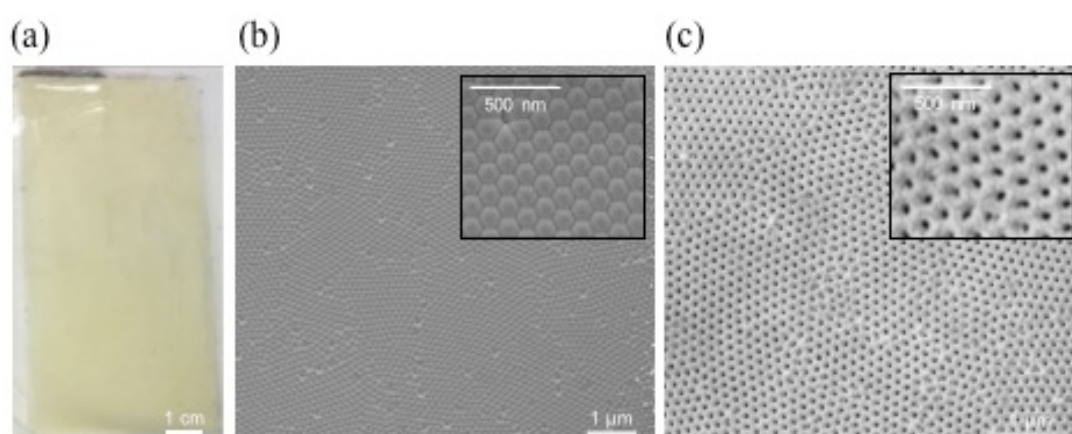


Figure 2.3 (a) Photograph and SEM micrograph of (b) NBDS substrates. After a 90 min. acid treatment, NCDS substrates displaying nanocratered topography can be obtained (c). The inset figures are higher magnification SEM images displaying the hexagonal packing of the nanopatterns.

In order to obtain the desired nanocratered topography for enhanced Raman signals (Figure 2.2.c), several acidic treatments were performed at different time intervals. Acidic solutions with different strengths were chosen to dissolve non-porous alumina of the nanobump decorated AAM barrier sides. The critical factor in creating the cratered structure was to increase roughness with increased curvature. Firstly, phosphoric acid was used to create nanocraters. Figure 2.4.a is the SEM image of the NBDS treated with 5% wt. phosphoric acid for 30 minutes. It was seen that the time was not enough to dissolve the top of the nanobump structures which enables the creation of the craters. The treatment time with 5% wt. phosphoric acid was further increased to 90 minutes (Figure 2.4.b). The non-uniform dissolution was observed with the increased treatment time. Partial over-dissolution was observed and the periodicity and the uniformity of the membranes were changed. Secondly, 5% wt. sulfuric acid treatment after 5% wt. phosphoric acid was performed as it was observed that the treatment with only phosphoric acid was not enough. Figure 2.4.c represents the topography of NBDS after immersed in 5% wt. phosphoric acid for 30 minutes followed by 30 minutes of 5% wt. sulfuric acid treatment. The desired topography also could not be achieved with this method because the acidic strength and the treatment time were not enough. Lastly the solution used for electropolishing the aluminum foil was used. 30, 90 and 120 minutes of etching intervals were performed with the electropolish solution and the SEM images of NBDS substrates after treatment were represented in Figure 2.4.d, e and f respectively. Figure 2.4.d and f represents under and over treatment with electropolish solution respectively. The desired nanocrater-decorated topography was observed in Figure 2.4.e which is obtained by 90 minutes immersion in the electropolishing solution (95% H_3PO_4 , 5 wt% H_2SO_4 and 20 g/mL CrO_3). As it can be seen from the SEM image, only the top of the nanobump structures were dissolved, yielding increased roughness and adequate curvature (see AFM images, in Figure 2.6 for more details).

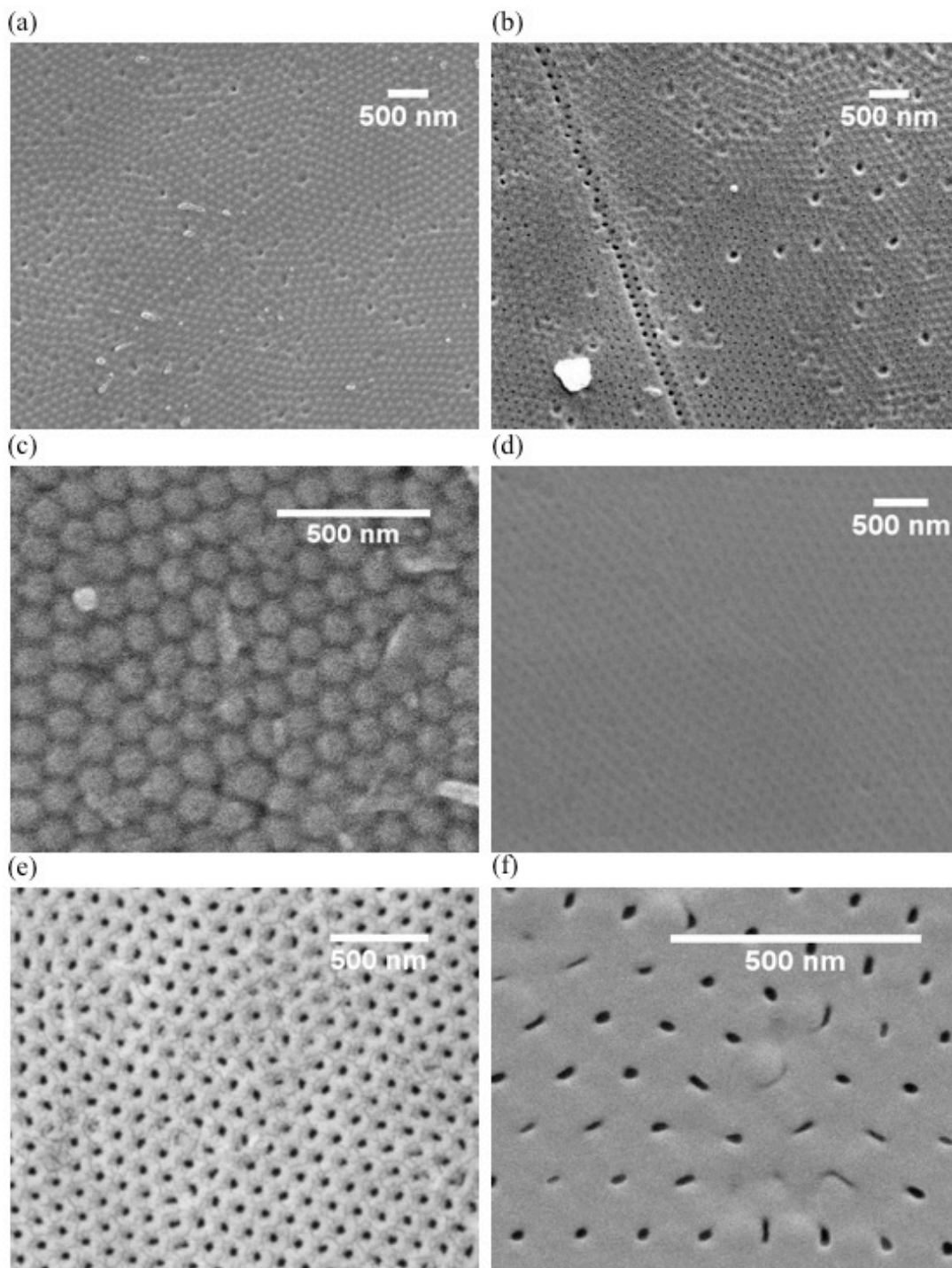


Figure 2.4 : SEM images of NBDS substrates treated with (a) 5% wt. phosphoric acid for 30 minutes, (b) 5% wt. phosphoric acid for 90 minutes, (c) 5% wt. phosphoric acid for 30 minutes followed by 30 minutes of 5% wt. sulfuric acid treatment, electropolish solution for (d) 30, (e) 90 and (f) 120 minutes.

The topographies of the produced NBDS and NCDS substrates were analyzed by image J software. The average diameter of the nanobumps and the nanocrater gaps were calculated by analyzing three independent samples (n=3) and found to be 130.79 ± 5.87 nm and 26.14 ± 3.18 nm, respectively. The diameter frequency distributions of both nanostructures were represented in Figure 2.5. The distributions of the average diameters were found relatively homogenous.

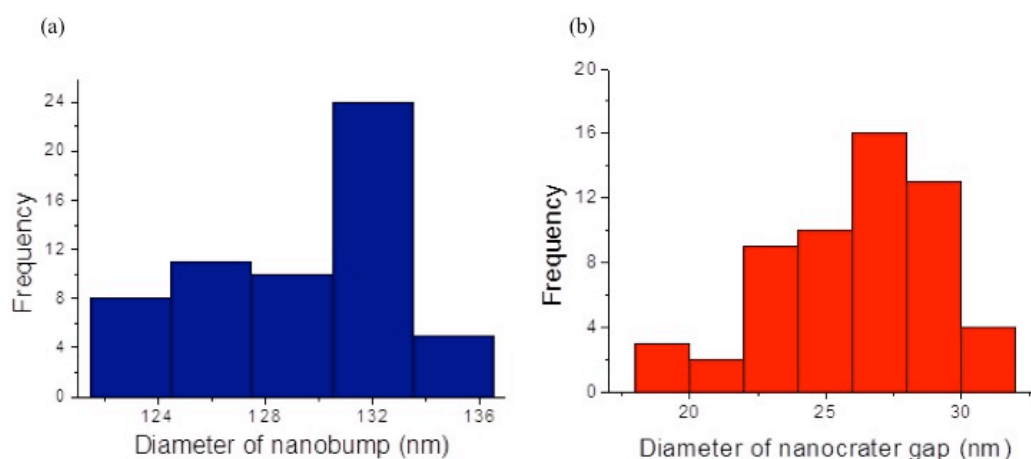


Figure 2.5 : Calculated diameter frequency distributions of (a) nanobumps of NBDS and (b) nanocrater gaps of NCDS.

NBDS and NCDS substrates' surface morphologies were also characterized by AFM in order to examine the 3-D topographies and roughness values. Figure 2.6 a and b shows the AFM images of NBDS and NCDS substrates respectively. The roughness values were calculated from AFM images by using its software. The roughness values of the 20nm-Au coated flat, NBDS and NCDS substrates were calculated as 1.2 ± 0.3 nm, 71.2 ± 7.2 nm and 152.1 ± 25.8 nm respectively. As the surface was treated with wet-etching, and nanobumps evolve into nanocraters, the roughness value increased dramatically. One of the aims of this research was to show the effect of increased roughness on the enhancement of the Raman signals besides from the increased curvature. These different roughness values would also create a change in the enhancement factor. Hence, the SERS signal intensities obtained from each sample will be different.

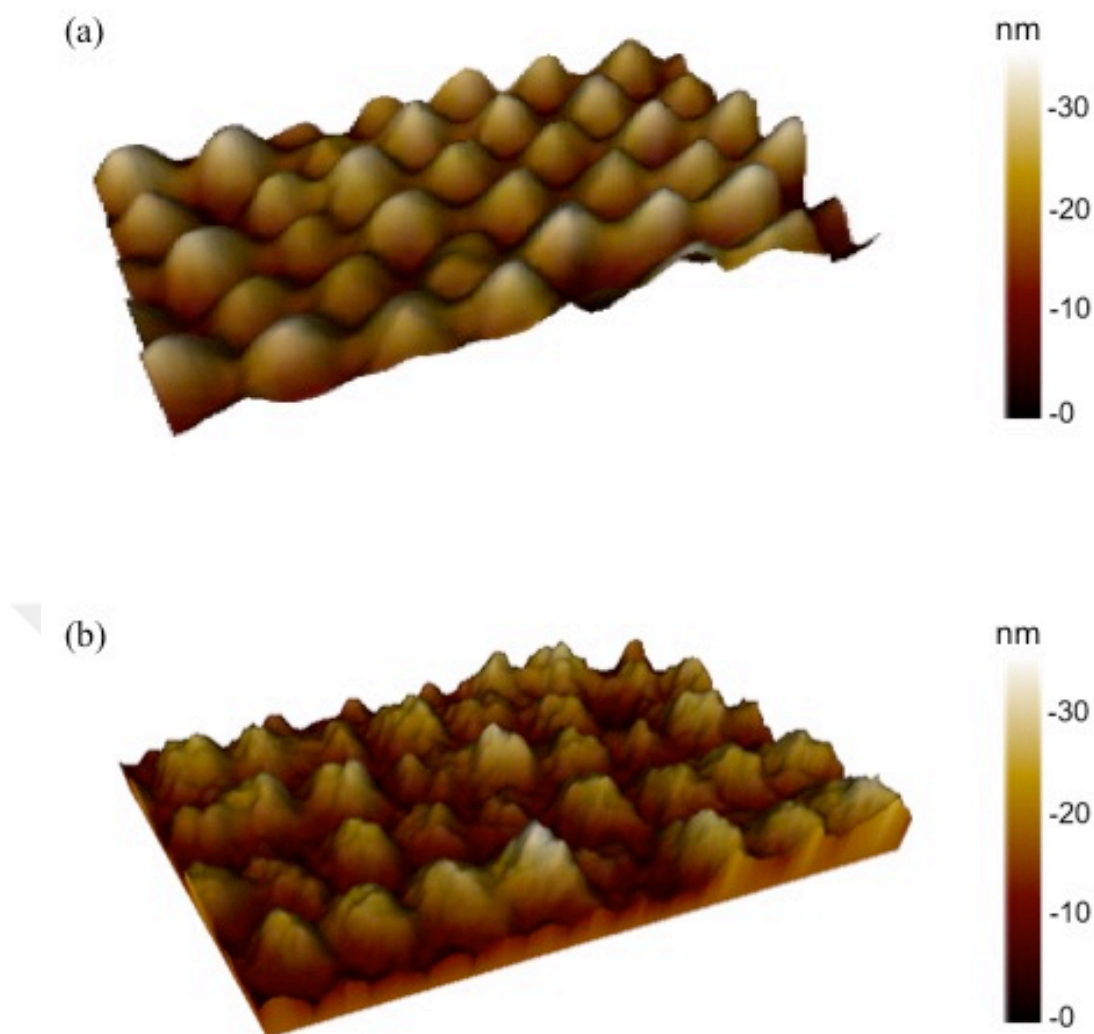


Figure 2.6 : AFM images of (a) 20 nm-Au@NBDS and (b) 20nm-Au@NCDS substrates.

The influence of metal coating thickness on the SERS intensity was examined by using MB on three different coating thicknesses for both fabricated surfaces. MB Raman intensities obtained from NBDS and NCDS substrates were shown in Figure 2.7. In both cases, for the detection of 10^{-3} M MB, 20 nm Au deposition provided higher signal intensities compared to 10 or 30 nm-thick Au coatings.

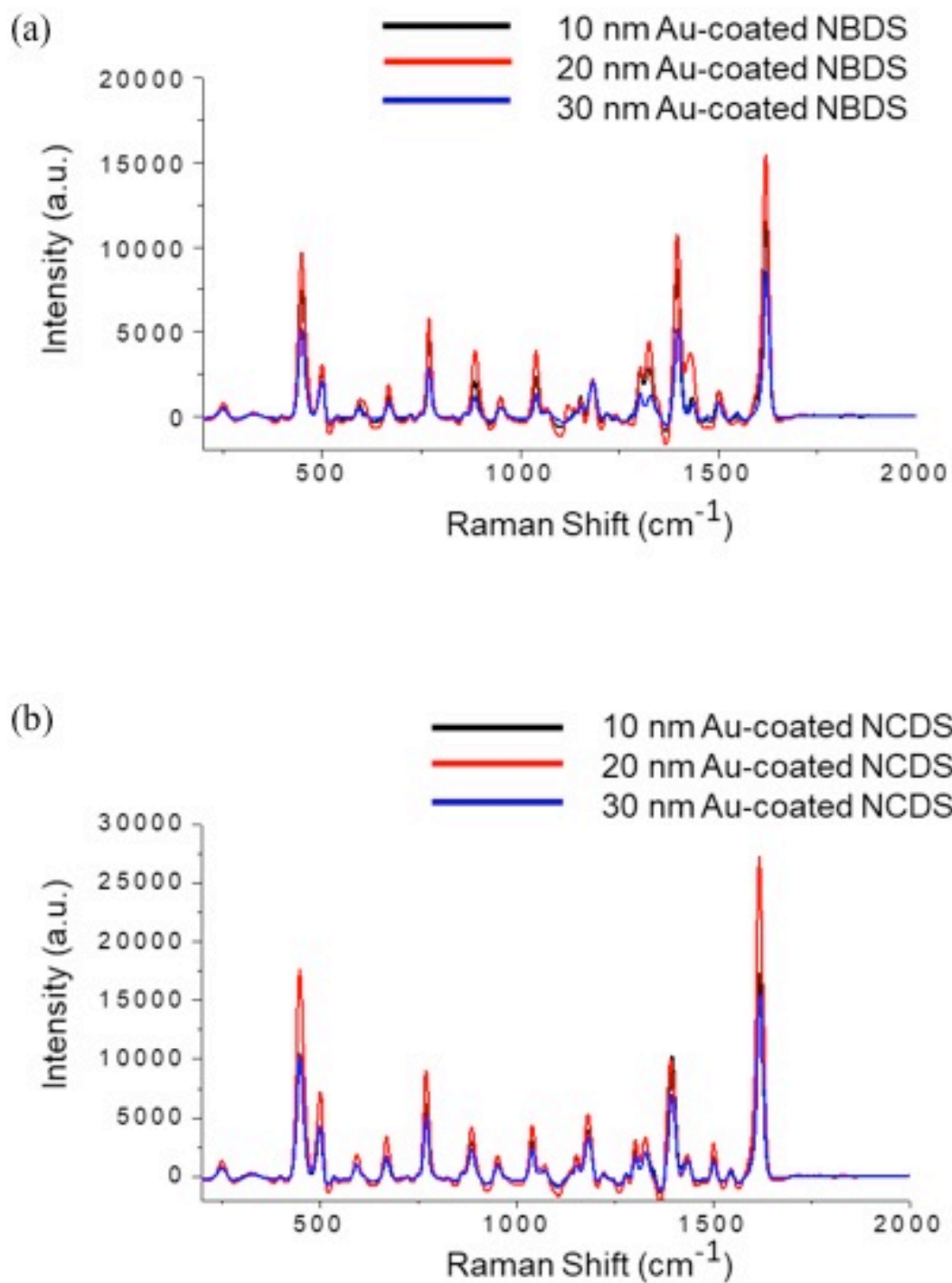


Figure 2.7 : MB SERS signals of 10^{-3} M MB obtained from 10, 20 or 30 nm thick Au-coated (a) NBDS and (b) NCDS substrates.

Although the collected Raman spectra have acceptable signal to noise ratios and show all signature MB peaks (Table 2.1), for inadequate metallic coating thicknesses, surface plasmon generation cannot be achieved effectively and weaker intensities were observed in the case of 10 nm coating thickness [52]. On the other hand, over coating of Au on the nanostructured surfaces leads to surface smoothing that translates into lowered enhancement efficiencies [53]. Thus, it was concluded that among the thicknesses investigated (10, 20, 30 nm), 20 nm Au coating allows highest SERS signal intensities for MB on both NBDS and NCDS substrates, and the following studies were conducted with 20 nm Au-coated samples.

Table 2.1 Experimental and literature values for some of signature Raman shifts of MB [49] and CR [54] dyes.

MB Raman Shift (cm ⁻¹)		CR Raman Shift(cm ⁻¹)	
Experimental	Assignments ^{xxxiii}	Experimental	Assignments ^{xxxiv}
1620	v(C-C)	1590	v(phenyl)
1436	vsym(C-N)	1409	v(N=N)
1394	vsym(C-N)	1281	v(phenyl-phenyl)
449	δ(C-N-C)	1157	v(phenyl-N)

Figure 2.8 illustrates the influence of surface topography on the SERS signals from MB (Figure 2.8.a) as well as CR dyes (Figure 2.8.b). 10⁻³ M of dye was detected in every measurement. For both Raman reporters, the Au@NBDS substrates (Roughness = 71.2 ± 7.2 nm) showed improved SERS intensities compared with Au@alumina coated silicon wafers (Roughness = 1.2 ± 0.3 nm) at the prominent Raman shifts of each molecule indicated in the literature from previous studies (Table 2.1). The signal enhancement on Au@NBDS substrates can be attributed to formation of the periodically ordered hotspots on the nanofeatured surface. The SERS signal intensity is dependent on the collective effect that appear on the surfaces with nanostructures in close proximity. The short-range interaction between periodically decorated nanostructures on Au@NBDS substrates reinforce the signal enhancement. The propagation of both localized and propagating surface plasmon resonances on the metal coated nanopatternes should also contribute the large difference between the SERS intensities [25]. The density of the hotspots and the

total effect of both surface plasmons determine the electromagnetic enhancement resulting in surface-enhanced Raman signals.

In the case of Au@NCDS substrates, collective effect of the nanostructures in close proximity, the density of the hotspots and the total effect of both propagating and localized surface plasmons contributes to the electromagnetic enhancement. More importantly, the increased roughness of the NCDS substrate (Roughness = 152.1 ± 25.8 nm), causes formation of hotspots with higher curvatures, yielding further signal enhancement for both dyes studied. The cratered geometry is also suspected to contribute to the formation of cavity resonance for the NCDS films. The larger SERS intensities for MB compared to CR were attributed to the higher chemical enhancement of this commonly used Raman reporter dye [50].

To substantiate these discussions and to model the formation of hotspots and demonstrate the electric field around the Au-coated nanobumps and nanocraters, computer simulations were performed by Comsol 5.0 Optics Module. For a realistic depiction of the surface topography SEM and AFM images of the corresponding surfaces were investigated and then, nanobumps were modeled as Au spheres with 65 nm radius, and nanocraters as Au tori with 65 nm outer and 13 nm inner radius in Comsol 5.0 Optics Module. Using finite element method, electric field generations were observed under 785 nm irradiation to simulate the experimental scenario.

The resultant electric field around a Au sphere with 65 nm radius (Figure 2.9.a) and a torus with 65 nm outer and 13 nm inner radius (Figure 2.9.b) were simulated as the corresponding constituent nanostructures of Au-coated NBDS and NCDS substrates respectively. The simulated electric field around the torus representing Au@NCDS was found to be higher than the electric field around the sphere representing Au@NBDS. The observed enhancement in the electric field around the torus is thought to arise from increased hotspot curvature and potential cavity resonance formation [55, 56], which causes the higher SERS intensities observed for the NCDS substrates compared to NBDS counterparts. This increase in the SERS enhancement on the NCDS substrate is thought to arise from this difference in the generated electric field around torus and sphere.

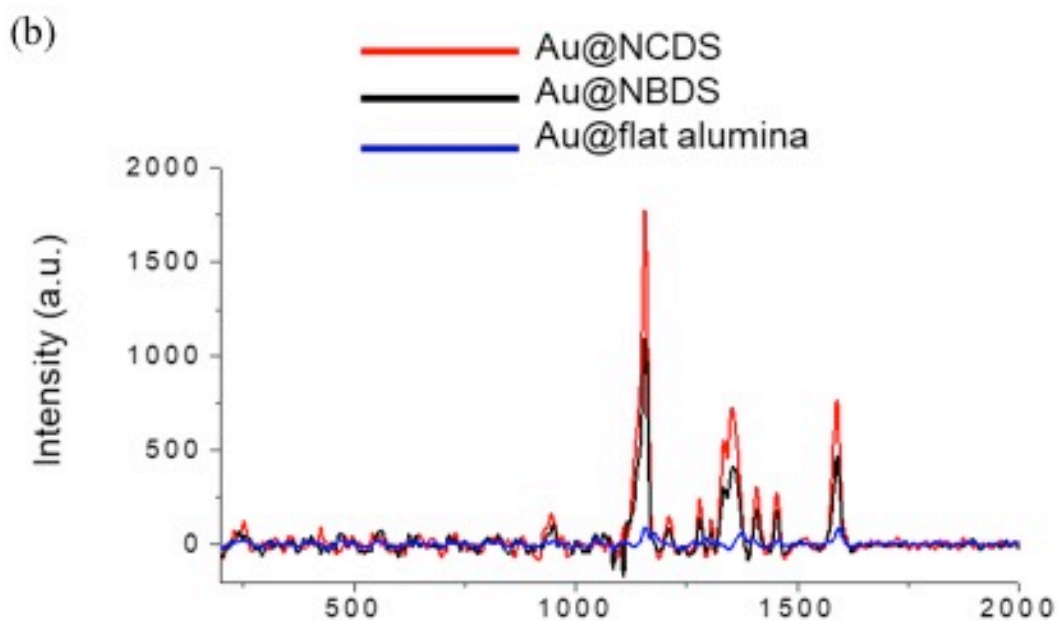
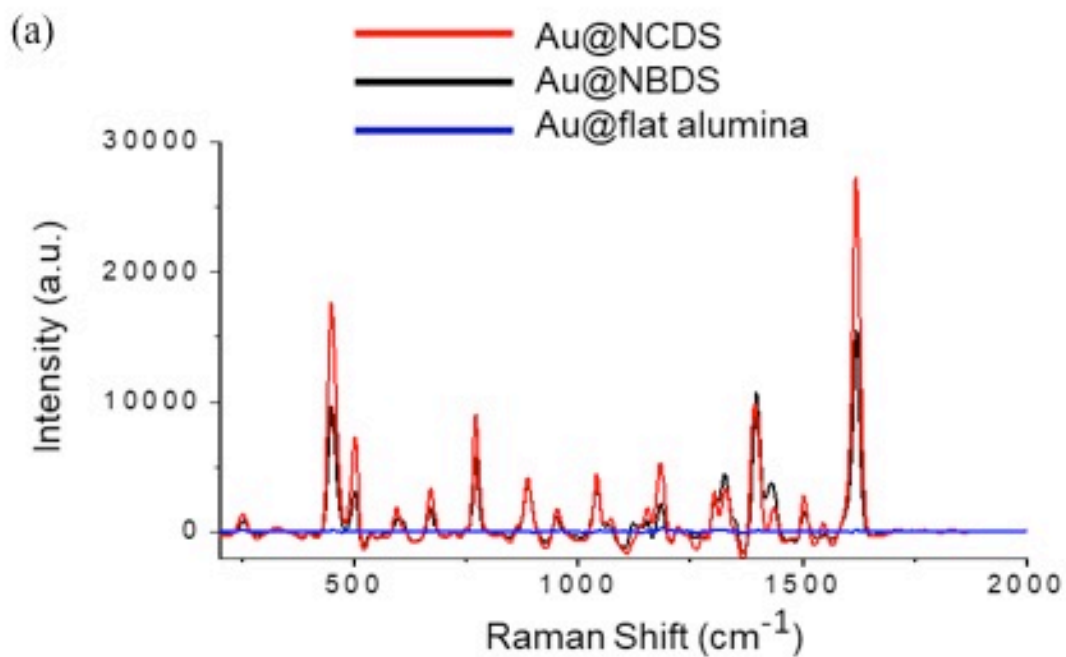


Figure 2.8 : (a) MB and (b) CR SERS signals obtained from NCDS, NBDS and Flat Alumina substrates after 20 nm Au coating.

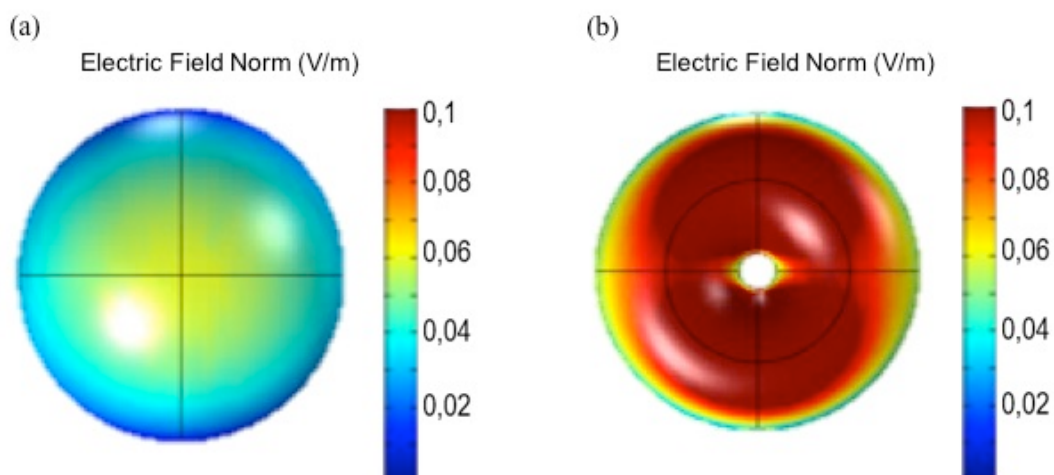


Figure 2.9 : Simulated electric field around the constituent individual (a) Au sphere (b) torus representing Au@NBDS and Au@NCDS substrates respectively.

A major limitation for SERS with regards to its common use for biosensing applications is the reproducibility of the enhanced signals [57]. This issue is especially more pronounced for colloidal nanoparticle systems where particle aggregation and variations in particle size causes irreproducible spectra because of the variations in the hotspot formation [58]. AAMs offer an economic and easy-to-synthesize platform for the non-litographic fabrication of plasmonic nanoparticle arrays with fine control over particle size, spacing and density with high periodicity and uniformity in a reproducible manner. In order to evaluate the potential of AAM-driven NCDS substrates as reproducible SERS platforms, 30 random locations from 3 independent samples were used, and the resultant spectra were presented in Figure 2.10.

Relative standard deviation (RSD) values for the signature peaks of MB were then calculated for quantification of reproducibility (Table 2.2). The average RSD value obtained from the Au@NCDS substrates was 0.117 for MB Raman shifts. More importantly, the RSD values lie below 10% for the most intense 449 and 1621 cm^{-1} shifts. This result can be considered as highly reproducible SERS data when compared with previous reports employing RSD calculations [49, 59].

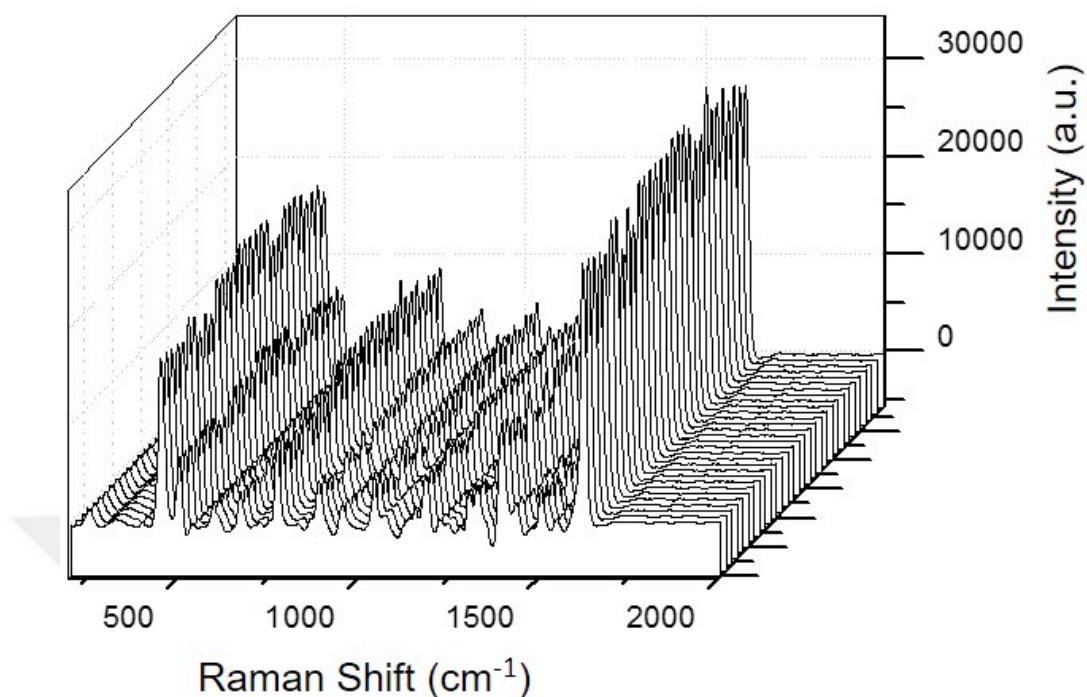


Figure 2.10 : SERS spectra of MB collected from 30 random spots of 3 independent Au@NCDS substrates.

Table 2.2 RSD values for the Raman shifts of MB collected from Au@NCDS substrates.

Peak Position (cm ⁻¹)	449	771	1184	1394	1436	1621
RSD Value	0,078	0,148	0,131	0,152	0,150	0,057

In the final part of the experimental study, limit of detection and EF calculations as well as durability experiments for the Au@NCDS substrates were conducted. Here, SERS spectra from series of different MB concentrations (10^{-3} M – 10^{-8} M) were collected on Au@NCDS substrates (Figure 2.11.a), and for control, MB (10^{-2} M) spectrum was obtained from Au-coated flat alumina samples. The spectra from NCDS substrates showed a gradual reduction with decreasing MB concentrations.

The lowest concentration yielding clear significant peaks was found as 10^{-7} M, and a linear signal reduction was observed between 10^{-4} and 10^{-7} M when the logarithm of MB concentration was plotted against the intensity of the most enhanced 1621 cm^{-1} signature peak (Figure 2.11.b). From this result, the LOD for MB on Au@NCDS substrates was found as 10^{-7} M, which is the minimum concentration that satisfies the linear trend [60]. The control SERS spectrum on the Au-coated flat alumina sample was then used to calculate the EF value for the periodically nanostructured NCDS substrates. By using the formula given in the methods section, EF was found as 2.3×10^5 for the nanocratered surface, which is comparable to previous reports that employed Ag-coated AAM-driven substrates [28, 61].

Finally, the SERS spectra of 10^{-7} M MB on fresh, 1-week and 1-month old NCDS substrates were taken to infer about the stability of the nanoplateforms. Figure 2.10 shows that the intensities of the signature peaks are very similar for samples with different resting periods (average RSD= 0.108), illustrating the durable nature of the Au@NCDS substrates.

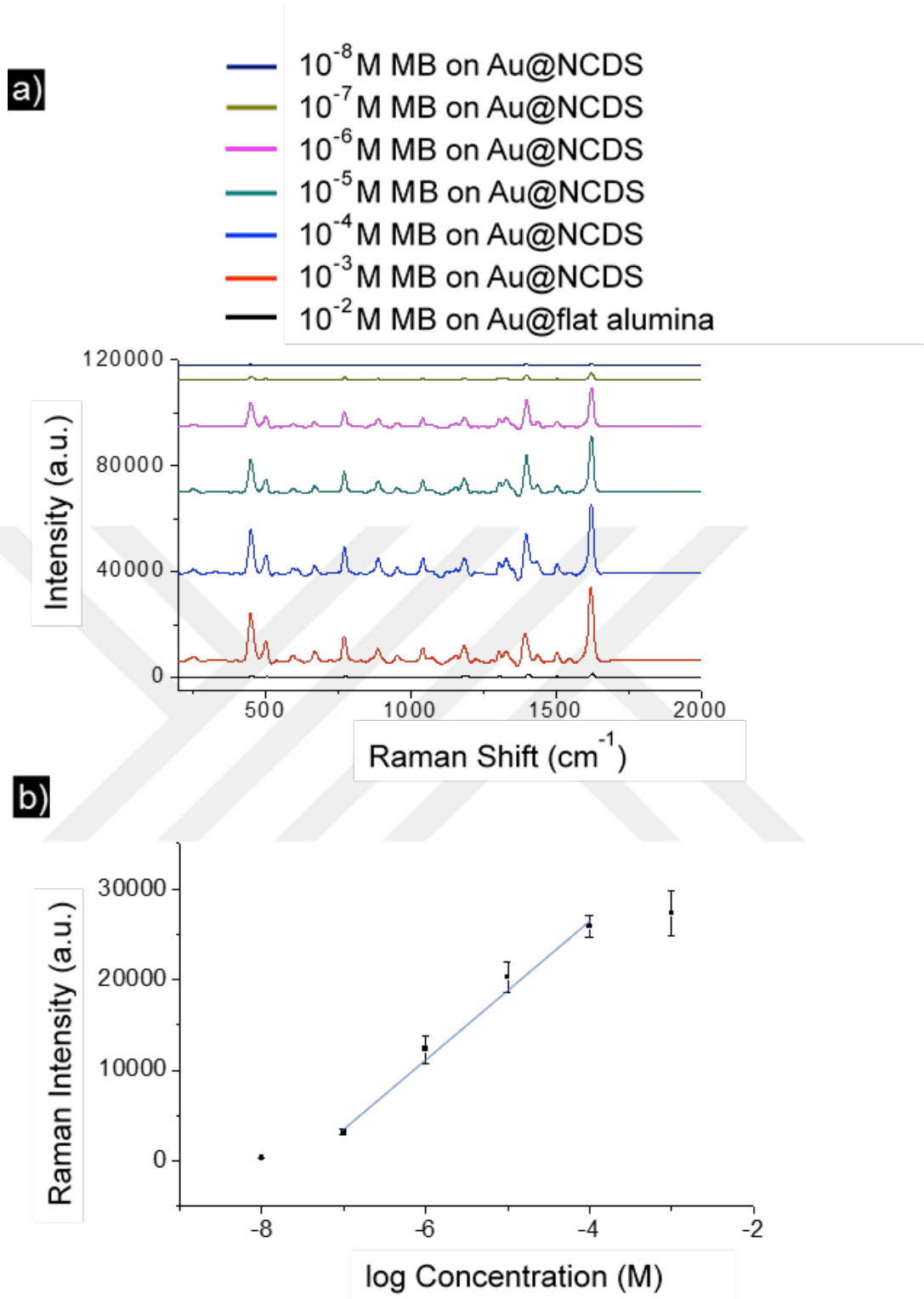


Figure 2.11 : SERS spectra of MB with different concentrations (a), and logarithm of MB concentration against the corresponding intensities at the 1621 cm^{-1} peak for Au@NCDS substrates (b). Straight blue line in (b) represents the linear region.

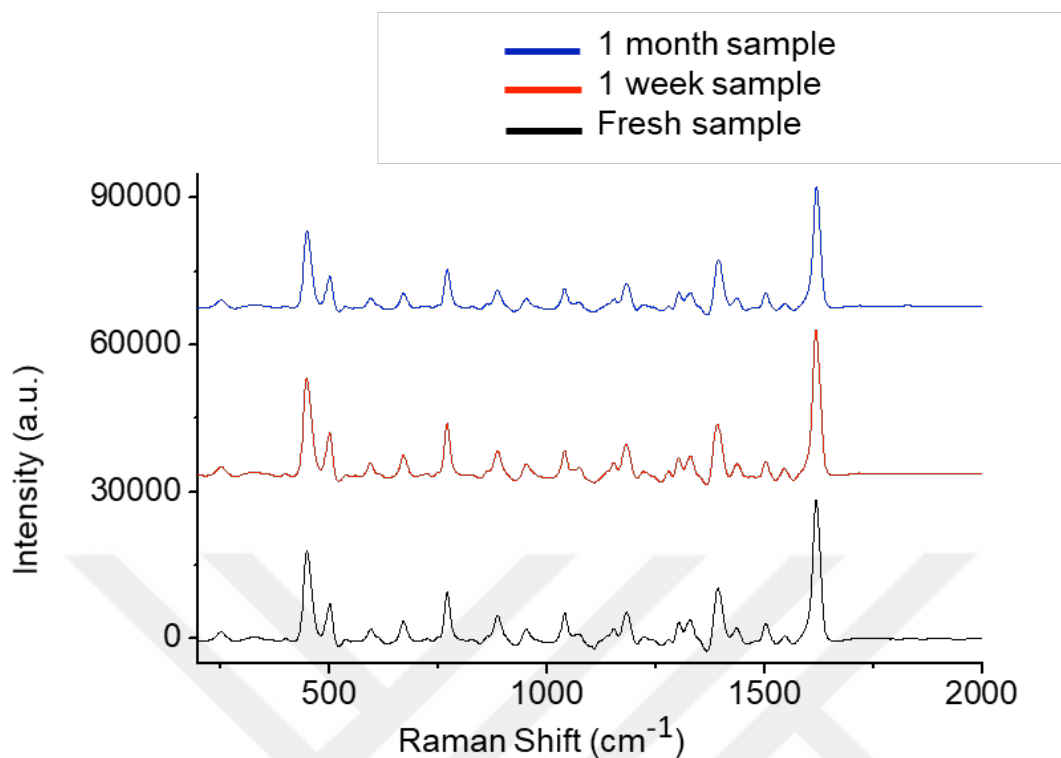


Figure 2.12 : SERS spectra of 10^{-3} M MB on Au@NCDS for different resting periods.

To sum up this section, nanobump-decorated barrier sides of AAMs were used as the base material for the non-litographic fabrication of plasmonic nanoparticle arrays with enhanced and reproducible SERS signals. The surface topography of such materials was altered by wet etching treatment to create the periodic nanocrater arrays, i.e., the NCDS substrates. After optimization of the Au thickness, NCDS substrates showed improved SERS intensities compared with the NBDS counterparts by using two different Raman reporters. This result was also confirmed with theoretical simulations, which showed the increased electric field on NCDS than NBDS substrate. Further studies with MB dye revealed that the Au@NCDS substrates were durable nanoplatoms that could provide reproducibly enhanced MB signals with LOD levels down to 10^{-7} M. The RSD values for obtained signals are $\sim 10\%$, which is accepted in literature as a suitable reproducibility in routine diagnostic applications. The durability values also show that this fabricated high-efficient surfaces could be stored and used for a long time period. These properties are required for an ideal SERS-active platform.

3. ANODIC ALUMINA MEMBRANES AS A MOLD FOR FABRICATING POLYMER-BASED SERS SUBSTRATES WITH TUNABLE PROPERTIES

3.1 Introduction

The main attention toward the fabrication of a SERS substrate is to find an easy, efficient and cost-effective technique that yields reproducibly strong SERS signals. AAMs offer a cost-effective way to obtain highly controlled nanostructured plasmonic arrays on a large scale (few cm² areas) compared with lithographic methods. Using AAM as a mold has a further advantage as it can be used repeatedly to obtain surfaces and further reduce the cost for obtaining prepatterned nanodecorated surfaces. It allows tuning the topography of the resultant films through changing the morphologic characteristics of the mold. For instance, pore size and pore depth can varied independently which translates into changes in diameter of the plasmonic particle and its length, respectively.

Polycarbonate is a commonly used thermoplastic for various purposes such as plastic lenses in eyewear, automotive components, protective gear and Digital Disks. It is a common and cheap polymer, with 155°C melting point. Durability and wide usage in optics and electronics also make it a commonly used polymer. Previous reports have revealed the use of AAMs as molds to obtain nanopillared polycarbonate substrates [62]. These surfaces with ordered nanofeatures could be obtained at large-scale and the control over mold properties directly affect topography of resultant polycarbonate surface.

After the report about polydopamine thin film coating on various surfaces [63], its usage gathered great attention due to its unique properties. Apart from its suitability of coating for almost all types of substrates, its ease, control over thickness and biocompatibility makes it attractive for creating functional surfaces. Polydopamine layer have chemical groups such as catechol, amine and imine. These groups not only serve as starting points for covalent modification for molecules, but also can be

used as a reducing agent for metal ions. With this unique property, polydopamine coating can be used as a platform for metallic nanoparticle reduction. The facile nature of the process has made this technique used as a common method for fabrication of several SERS substrates [49, 64].

3.1.1 Adjusting the mold topography

As SERS is highly surface dependent, surface topography is the prominent factor on signal enhancement. AAM's main advantage is its highly controllable topography through varying anodization parameters. Changing the parameters such as anodization voltage and electrolyte type will influence the pore structure and arrangement, which in turn, alter the topography of the obtained plasmonic surfaces as well as their packing density and ordering on these molds will change.

In particular, by changing the duration of the pore widening wet etching step, the diameters of the pores change. Longer treatment time causes wider pores, without changing the interpore distances. Using these AAMs with different pore sizes as molds for creating nanostructure decorated polycarbonate surfaces causes different nanostructure sizes with same structure-to-structure distance. Moreover, as mentioned in the previous sections, the hexagonally packed uniform porous structure allows fabrication of PC nanopillar arrays spanning about 50 cm² total areas.

3.1.2 Aim

The aim of this part of the thesis is to demonstrate the use of AAMs as a mold for fabricating PC-based SERS substrates displaying tunable signal characteristics. In creating the plasmonic particles, the drop-casted nanopillar decorated PC surfaces are coated with a simple polydopamine initiated Ag reduction scheme instead of the previously reported costly metal evaporation [62]. The control over plasmonic properties were intended to be satisfied through using molds with different pore diameters but same pore-to-pore distance. This was achieved by varying the pore widening step after two-step anodiation.

3.2 Experimental

3.2.1 Materials

High purity Aluminum foils (99.999%, Puratonic, 1 mm thickness) and Methylene Blue (MB) were purchased from Alfa Easer. Silver nitrate, dopamine HCl, acetone, dichloromethane, PC, hexane, HCl, H₂SO₄, NaOH, H₃PO₄ and C₂H₂O₄ were obtained from Sigma Aldrich. CrO₃ was purchased from Prolabo and Octadecyltrimethoxysilane was obtained from Acros Organics. Deionized (DI) water (18 MΩ) was obtained from a Thermo Scientific Smart2pure system.

3.2.2 Methods

3.2.2.1 Fabrication of AAMs

Nanoporous AAMs were prepared by two-step anodization method [11]. High purity aluminum foil (99.999%) was sanded with 600 grit sand paper and sonicated in water. Further sonication with acetone was performed in order to get rid off the organic residuals. The foil was then electrochemically polished using a Pb cathode in an acidic solution (95% H₃PO₄, 5 wt% H₂SO₄ and 20 g/mL CrO₃) under 15 V at 65 °C for 90 minutes. Electropolished foils were anodized using 0.3 M oxalic acid as electrolyte against stainless steel at 5 °C under 50 V for 15 hours in the first anodization. The non-uniform alumina (Al₂O₃) layers formed on the both sides of Al foil were then removed using 0.4 M H₃PO₄ and 0.2 M CrO₃ solution at 75 °C. A second anodization step was applied for 163 second with the same conditions as in the first one to obtain AAO films with periodically ordered hexagonal nanopores on both sides of the aluminum foil with 300 nm thickness. In order to adjust the pore sizes to approximately 80 and 100 nm, 45 and 52 minutes of 5% (w/v) H₃PO₄ treatment to the AAMs were performed respectively.

3.2.2.2 Hydrophobic coating on AAMs

In order to achieve hydrophobic molds that easily release the molded PC films, AAMs were incubated in 0.05%(v/v) ODTs in hexane for overnight. After the incubation, membranes were kept at 90°C for 4 hours. To check the hydrophobic characteristic of the membranes, contact angle measurements were performed by

using Biolin Scientific, Attension Optical Tensiometer from 3 independent silane-modified AAMs.

3.2.2.3 Fabrication of nanopatterned PC films

PC solution was prepared in dichloromethane solvent at 6% (w/v) concentration. The polymer solution was then drop-casted on ODTS-coated AAM. The PC solution on the AAM was kept at room temperature overnight. The dried film was then carefully peeled off from the membrane surface. (Fig. 3.1)

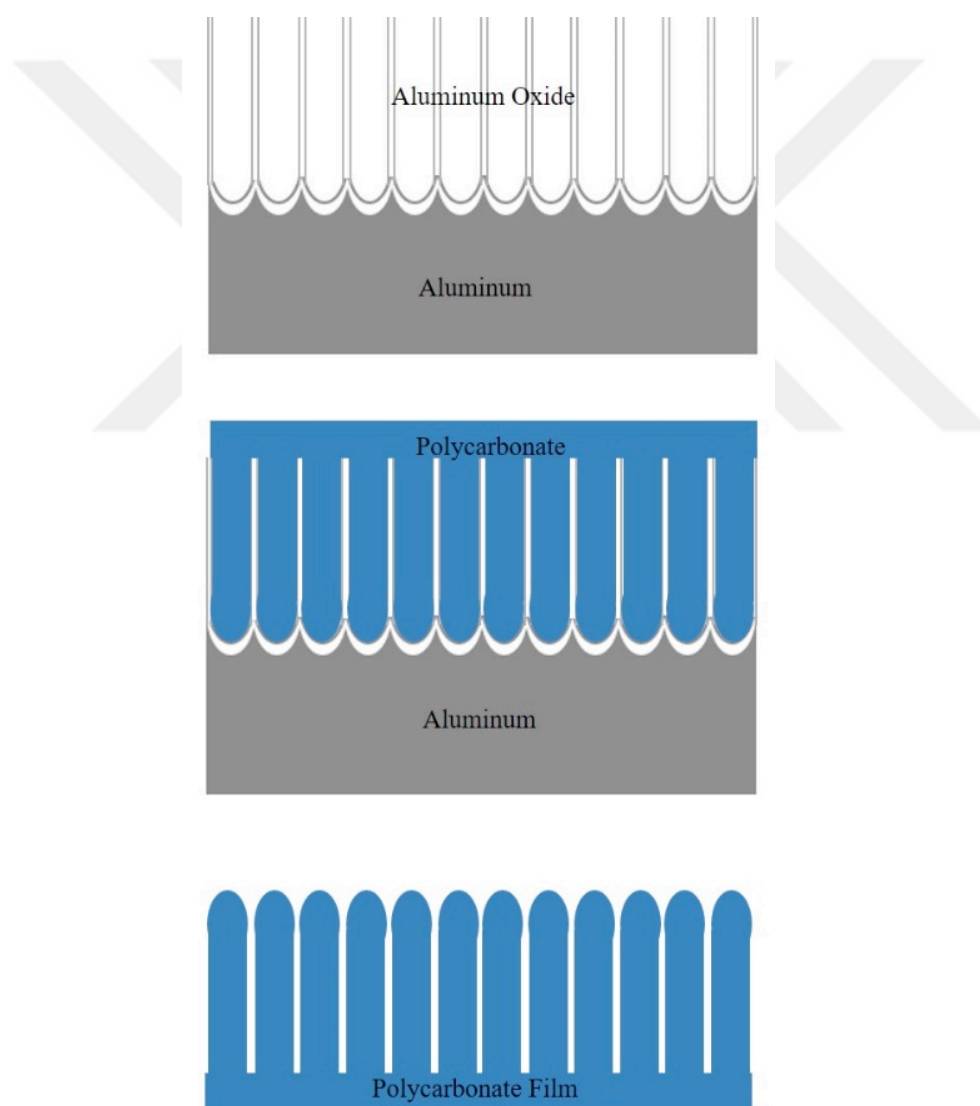


Figure 3.1 : Schematic representation of the fabrication of nanopatterned PC films by using hydrophobically-modified AAM molds.

In order to investigate the effect of nanopillar topography on Raman signal intensity, flat PC substrates were also fabricated for control. Same PC solution was drop-casted on ODTS-coated silicon wafer. The PC solution on the AAM was kept at room temperature overnight. The dried film was then carefully peeled off from the wafer surface.

3.2.2.4 Dopamine coating to PC films and silver deposition

The fabricated surfaces were immersed into 2 mg mL^{-1} in 10 mM Tris buffer (pH=8.5) dopamine solution at room temperature for 3 hours [49]. The surfaces then rinsed with water. For silver nanoparticle formation, polydopamine coated surfaces were treated with 50 mM silver nitrate solution in water for 24 hours to deposit metallic silver on the polydopamine coating. After treatment, the surfaces were rinsed with water and dried with N_2 gas.

3.2.2.5 Characterization of the produced platforms

Morphological characterization of the substrates were conducted by environmental scanning electron microscopy (SEM) (ESEM, FEI, Quante 200, 15 kV accelerating voltage).

3.2.2.6 SERS sample preparation and SERS measurements

MB was used as the Raman reporter to evaluate the SERS performances of the fabricated surfaces. $3 \text{ }\mu\text{L}$ aqueous solution of the Raman reporter was dropped on a $\sim 1 \text{ cm} \times 1 \text{ cm}$ silver-reduced surface and the surface was kept in dark at room temperature until the Raman reporter dried. SERS measurements were collected with a Raman system (DeltaNu Examiner Laramie, WY, USA) using a cooled charge-coupled detector (CCD) in the range of $200\text{-}2000 \text{ cm}^{-1}$ with 785 nm laser source. The measurements were done with 20 x objective, $3 \text{ }\mu\text{m}$ laser spot size, 60 s acquisition time and 150 mW laser power.

3.2.2.7 Computational simulations

In order to determine the formation of hotspots and demonstrate the electric fields on the metal-coated nanopillars with two different diameters, simulations were performed by Lumerical FDTD Solutions. After investigation of the SEM images,

the nanostructures were modeled. Using finite element method, electric field generations on the surfaces under 785 nm irradiation were simulated.

3.3 Results and Discussion

In the first part of this study, AAMs with two different pore sizes were fabricated. The incubation time of the AAM in 5% (w/v) H_3PO_4 determines the pore size. According to previous trials in our lab, it is known that in order to open the pores to ~ 80 nm, 45 minutes of incubation, and to open ~ 100 nm, 52 minutes of incubation is required [65].

Following pore widening step with acidic treatment, ODTS coating was performed in order to reduce surface energy and to be able to peel the polymer layer off the surface easily. The calculated contact angle for ODTS coated AAM is $132,07 \pm 2,80^\circ$. (Fig 3.2)



Figure 3.2 : Photograph from contact angle measurement of AAM after ODTS coating.

As the AAMs could be obtained in large areas (~ 50 cm²), nano-decorated PC surfaces could also be fabricated as wide as 50 cm². The fabricated nanopillar decorated PC surfaces are shown in Figure 3.3. Here, the PC surfaces obtained from AAMs with 80 nm pores are named as small nanopillar PC (SNPC), whereas films from AAM molds with 100 nm pores are named as large nanopillar PC (LNPC).

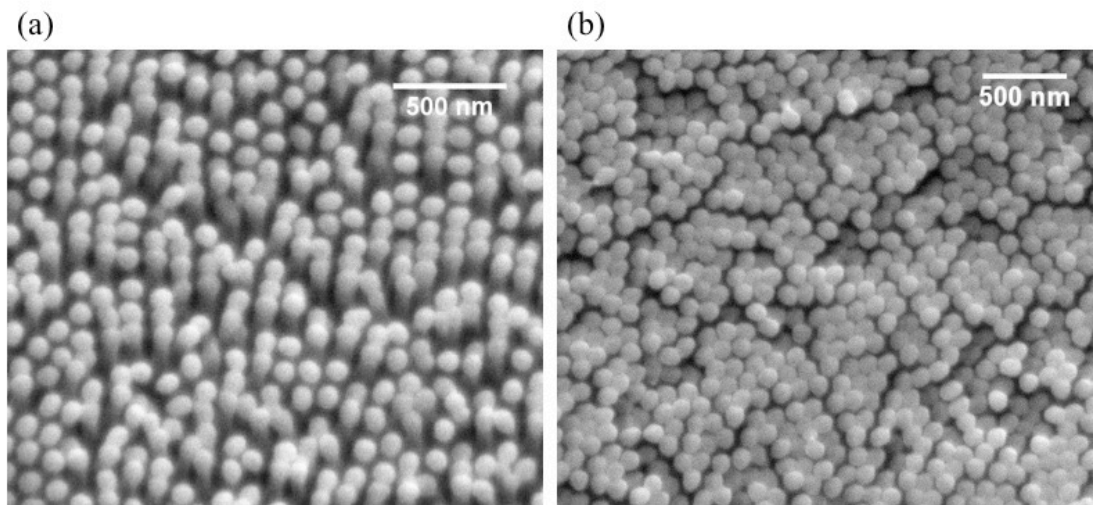


Figure 3.3 : SEM micrograph of (a) SNPC and (b) LNPC substrates.

The pillar sizes of the produced surfaces from two different molds were analyzed by image J software. The average pillar diameters on the SNPC and LNPC substrates were calculated by analyzing three independent samples ($n=3$) and found to be 81.20 ± 4.06 nm and 107.12 ± 5.88 nm, respectively. The resultant diameters are in line with the pore sizes of the starting AAM molds as expected, the diameter frequency distributions of both nanostructures were represented in Figure 3.4. The distributions of the average diameters were not wide and can be considered as relatively uniform.

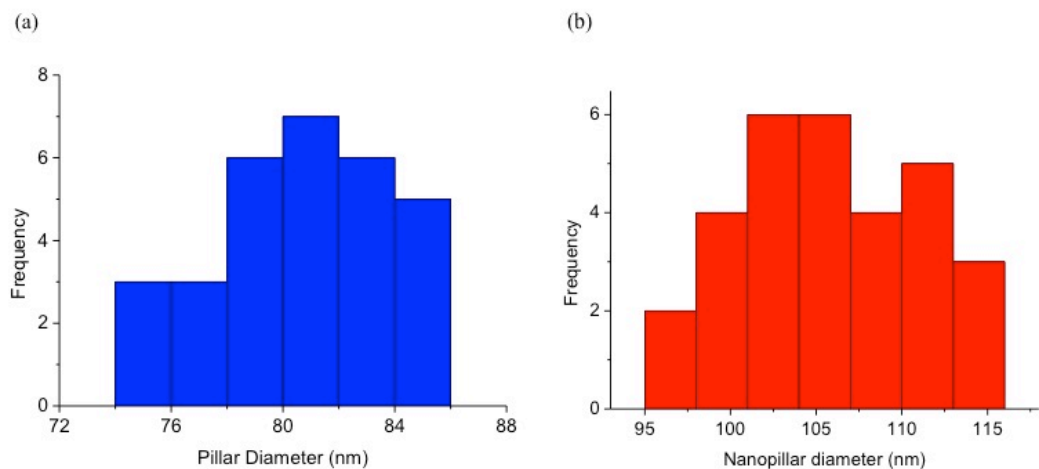


Figure 3.4 : Calculated diameter frequency distributions of (a) SNPC and (b) LNPC substrates.

Polydopamine coating on the fabricated surfaces were performed. Surfaces were incubated in 2 mg mL^{-1} dopamine HCl solution in water for 3 hours. The surface topographies of SNPC and LNPC surfaces after polydopamine coating are represented in Figure 3.5 a and c respectively. Polydopamine coating caused nanopillars to form groups with decreased pillar-to-pillar distance. Because SNPC substrates have smaller pillar sizes, gaps were formed as pillars came together. On the other hand, pillars on LNPC substrates came together and formation of tiny junctions between nanopillar groups were observed.

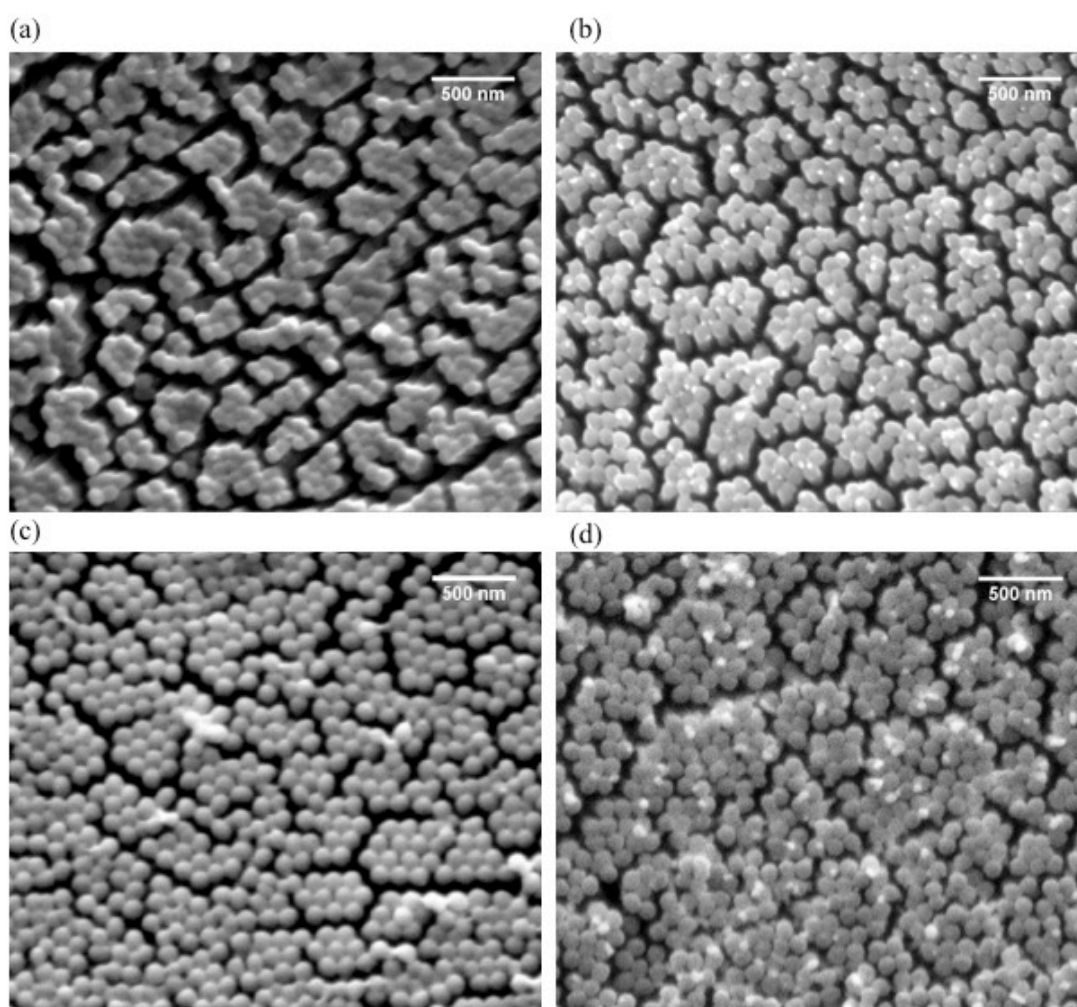


Figure 3.5 : SEM micrographs of polydopamine coated (a) SNPC and (c) LNPC substrates and after 24 hours of silver deposition on (b) SNPC and (d) LNPC surfaces that have been polydopamine-coated.

In order to examine plasmonic effects, silver reduction was performed on both surfaces followed by polydopamine coating. It has been reported that polydopamine can reduce metal ions and SERS platforms on various polydopamine coated surfaces can be obtained [64]. Polydopamine coated SNPC and TNPC substrates were incubated in 50 mM AgNO₃ solutions for 24 hours and Figure 3.5 c and d are the SEM graphs of Ag NP@TND and Ag NP@LND respectively.

Figure 3.6 illustrates the influence of PC nanopillar size, i.e. varying mold topography on the SERS signals from MB. 10⁻³ M of dye was detected in every measurement. Ag@LNPC polycarbonate substrate showed improved SERS intensities compared with Ag@SNPC polycarbonate substrate at the prominent Raman shifts of each molecule indicated in the literature from previous studies (Table 2.1). The signal enhancement on both substrates compared to flat PC can be attributed to formation of the periodically ordered hotspots on the nanofeatured surface. This surface provides an ideal platform for the subsequent Ag deposition which converts the ordered arrays of polymer nanopillars to periodic plasmonic antennas, the collective affect of which causes the observed increase for the LNPC and SNPC substrates. The non-negligible signal from the flat-PC substrate is originating from the deposition of Ag in nanoparticle form that also can act as plasmonic particles and enhance the Raman signal of the reporter dye.

The SERS signal intensity is dependent on the collective effect that appear on the surfaces with nanostructures in close proximity. The incident radiation causes an excitation of plasmons trapped between two closely arranged nanostructures, therefore a huge electric field between nanopillars occur. As pillars on LNPC are more closely packed to eachother, enhancement on this surface is higher compared to SNPC surfaces.

To substantiate these discussions, formation of hotspots and electric field around the nanopillars, computer simulations were performed by Lumerical FDTD Solutions. (Figure 3.7) In simulations constituents of SNPC surfaces were modeled as two Ag spheres with 40,5 nm radius and constituents of LNPC surfaces as spheres with 53,5 nm radius. The pillar-to-pillar distance was chosen as 250 nm and this is translated from the pore-to-pore distances of AAMs. As can be seen in Figure 3.7, the extend of hotspot formation and strength of electrical field is much higher for the more closely packed LNPC surface when compared to the SNPC counterpart. This larger electric

field generation should be the reason for the increased SERS signals for LNPC substrates observed in Figure 3.6.

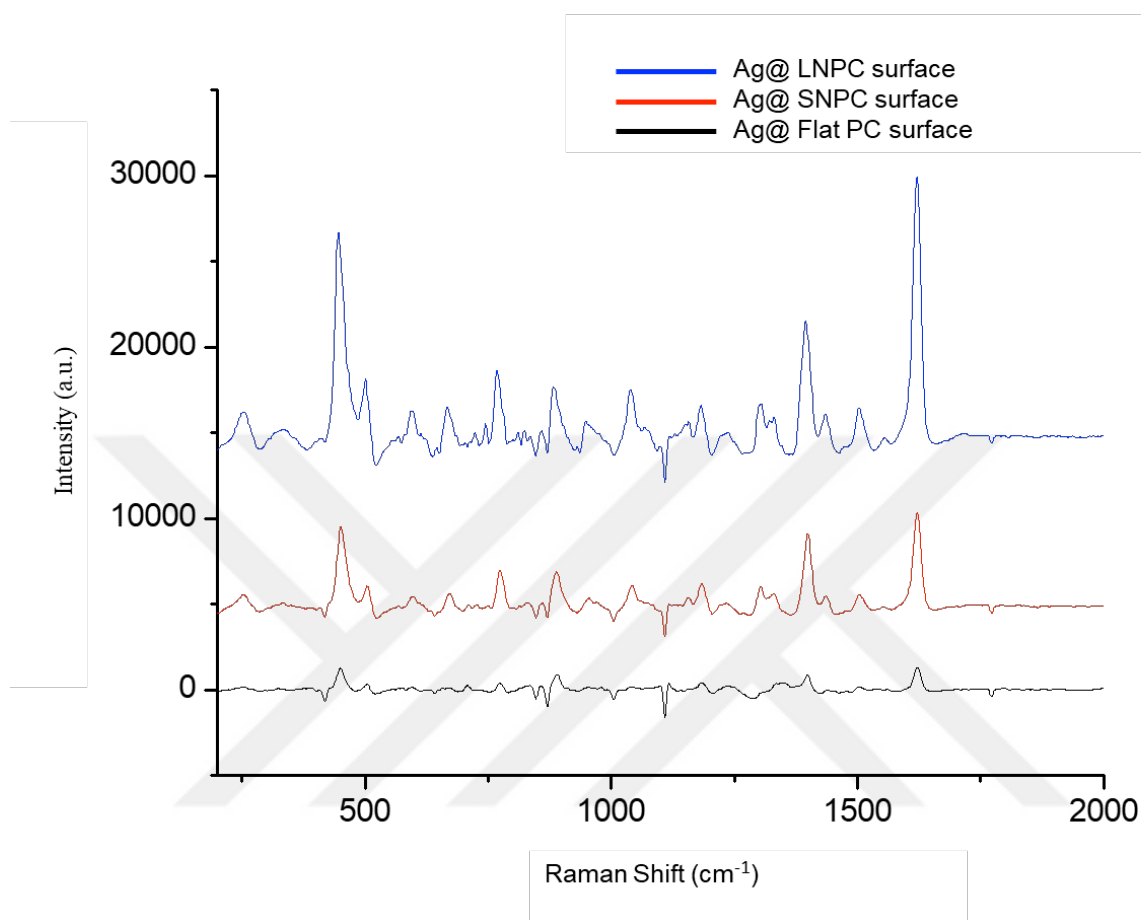


Figure 3.6 : MB SERS signals from Ag deposited SNPC (black) and LNPC (red) polycarbonate surfaces.

In order to infer about the reproducibility of the obtained SERS signals nanopillared substrates, relative standard deviation (RSD) values for the signature peaks of MB were calculated for the substrates with higher signal quality (Table 3.1). The average RSD value obtained from the Ag@LNPC substrates was 0.118 for MB Raman shifts. More importantly, the RSD values are $\sim 10\%$ for the most intense 449 and 1621 cm^{-1} shifts. This result can be considered as highly reproducible SERS data when compared with previous reports employing RSD calculations [49, 66].

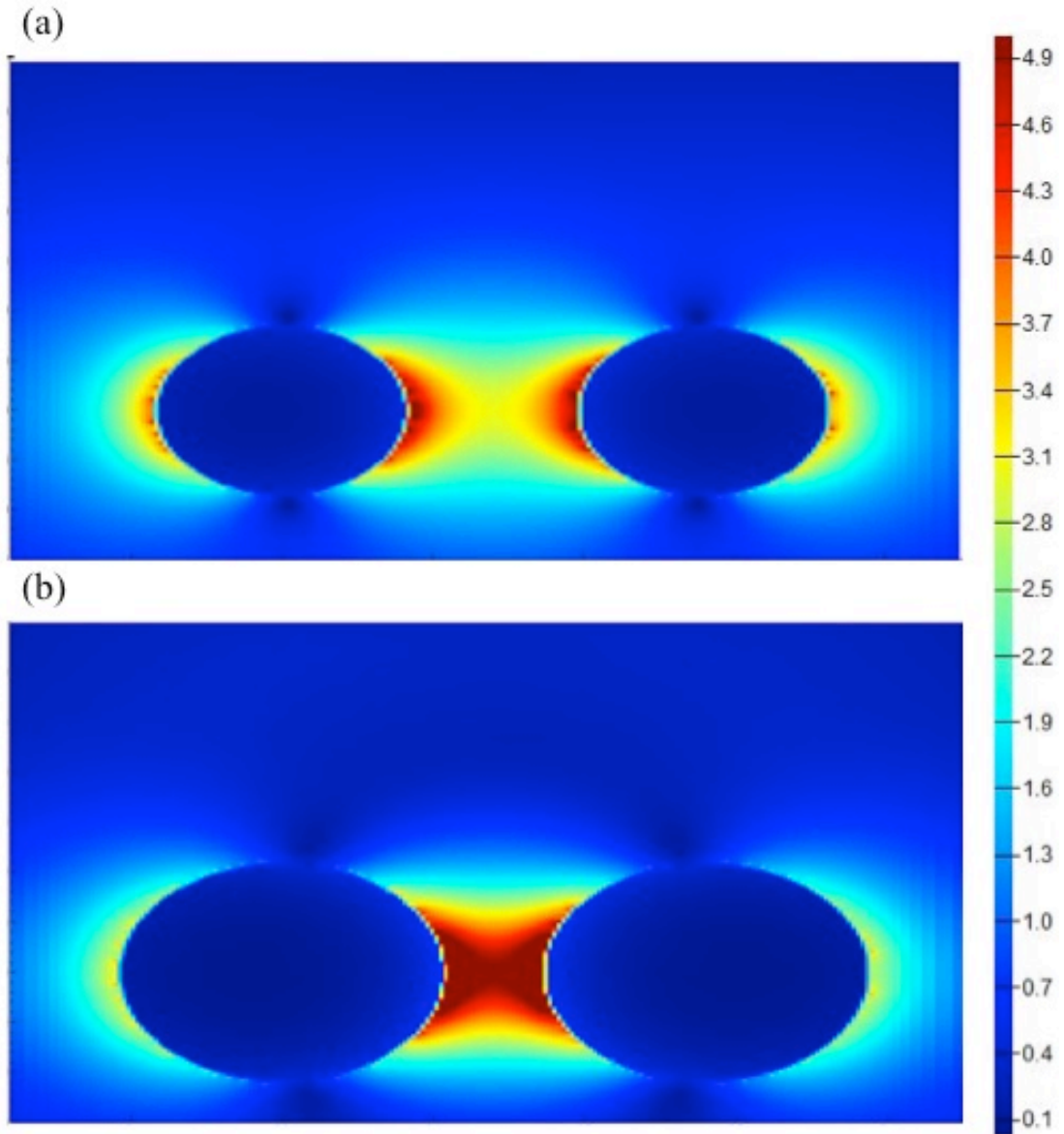


Figure 3.7 : Simulated electric field around the constituent two adjacent Ag spheres with (a) 40,5 nm radius and (b) 53,5 nm radius representing Ag@SNPC and Ag@LNPC substrates respectively.

Table 3.1 : RSD values for the Raman shifts of MB collected from Ag@LNPC substrates.

Peak Position (cm^{-1})	449	771	1184	1394	1436	1621
RSD Value	0,111	0,131	0,093	0,092	0,186	0,097

In the final part of this section, the effect of the Ag deposition time was investigated by using LNPC substrates. Samples (n=3, 5 spots from each) were treated with different Ag deposition times varying from 3 hours to 7 days and then the corresponding SERS spectra were collected. The results are depicted in Figure 3.8. As the deposition proceeds from 3 hours to 24 hours, a continuous Ag deposition on PC surfaces without losing the base topography occurred. The size and the density of the Ag nanoparticles increases from 3 hours to 24 hours, therefore closer and denser nanoparticles causes higher local electric fields. Especially when the distance between nanoparticles d , is further decreased down to the diameter of nanoparticles, 10^5 signal enhancement could be obtained due to the collective oscillation [56]. Further increase in the Ag deposition times to 48, 72 hours and 1 week gradually causes the surface topography smoothening. Therefore, nanostructured surface started to be degenerated, causing a decrease in the SERS enhancement due to the loss of surface plasmons. As it can be seen from Figure 3.8, maximum SERS signal intensity can be obtained from 24 hours Ag deposited LNPC.

To sum up, in this section AAMs were used as a mold for the non-litographic fabrication of plasmonic nanoparticle arrays with enhanced and reproducible SERS signals. The surface topography of the polycarbonate nanostructured surface was adjusted by changing pore sizes of AAM mold. By using two different pore sizes, two surfaces with different nanopillar diameters were obtained without changing pillar-to-pillar distance. As a trivial method for obtaining plasmonic nanostructured arrays, nanoparticle reduction was performed. Polydopamine coating was used as a reducing agent for silver ions. After Ag ion reduction for 24 hours, Ag@LNPC and Ag@SNPC substrates were obtained. Ag@LNPC substrates showed improved SERS intensities compared with the Ag@SNPC counterparts by using Methylene Blue as Raman reporter. This result was also confirmed with theoretical simulations, which showed the increased electric field on LNPC than SNPC substrate. Ag@SNPC substrates provided reproducibly enhanced MB signals with RSD values $\sim 10\%$.

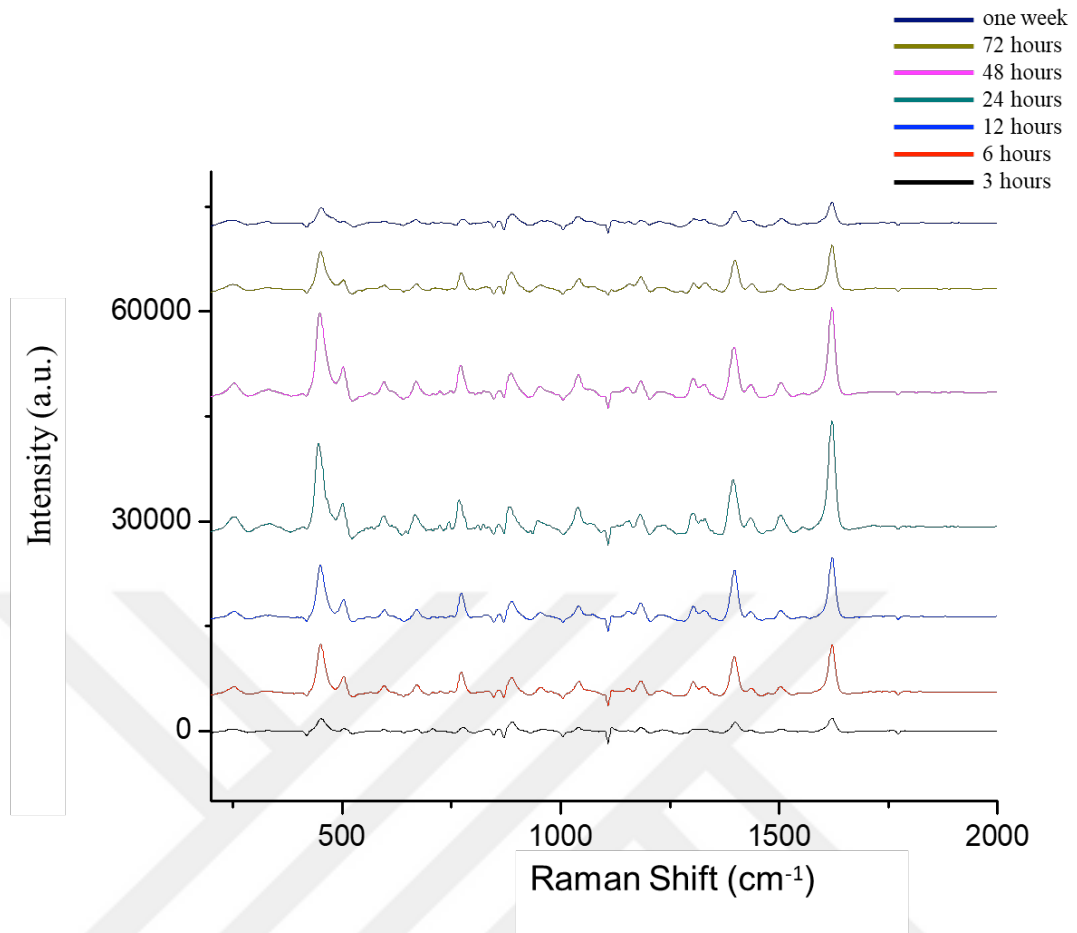


Figure 3.8 : MB SERS spectrum from LNPC substrates with different Ag deposition times



4. CONCLUSION

AAMs are hexagonally arranged arrays of nanopores obtained from anodization of high purity aluminum. Due to their controllable pore structures and porosities by optimizing anodization conditions, AAMs have intensively been studied for developing SERS substrates.

In the first part of the study, gold evaporated periodically nanobump decorated barrier side of AAMs are used as a SERS substrate. With this technique plasmonic nanostructured arrays could be obtained reproducibly and the topography is highly controlled and periodic. Compared with lithographic techniques, fabrication of AAMs are cost-effective and could be applied to large scales. The closely packed nanobump structures cause dense hotspots in between and the continuous gold coating induces propagating surface plasmons resulting in highly enhanced electric field around nanostructures. The periodicity of nanostructures provides reproducibility of SERS signals obtained from these surfaces with low spot-to-spot difference. Further modification on the nanobump decorated surfaces (NBDS) are performed to form nanocrater decorated surfaces (NCDS). With the cavities that are obtained with NCDS substrates and with the increased roughness compared to NBDS, higher electric field enhancements thus higher SERS signal intensities were achieved.

In the second part of the study, AAMs were used as mold for the non-lithographic fabrication of polymer-based plasmonic nanoparticle arrays. The control over the mold topography enables us to control the surface topography of the PC nanostructured surfaces. By using two different molds with different pore sizes by changing the simple pore widening process, two surfaces with different nanopillar diameters were obtained without changing pillar-to-pillar distance. Polydopamine coating was used as a reducing agent for silver ions for obtaining a facile method for fabricating plasmonic nanopatterned surfaces. After Ag ion reduction for 24 hours, Ag@LNPC and Ag@SNPC substrates were obtained. Ag@LNPC substrates showed improved SERS intensities compared with the Ag@SNPC counterparts by using

Methylene Blue as Raman reporter. This result was also confirmed with theoretical simulations, which showed the increased electric field on LNPC than SNPC substrate.

SERS can not be used as a routine detection tool because of its reproducibility problems. In order to obtain reproducibly strong SERS data, two different approaches for fabricating SERS substrates from AAMs were employed as a non-lithographic fabrication of robust SERS substrates displaying plasmonic nanoparticle arrays for routine diagnostic analysis for SERS.



5. FUTURE WORKS

The studies for fabricating aluminum-free hexagonally-packed pore structured alumina membranes are focused on to decrease its thickness to sub-micron levels. These ultra-thin AAMs with a thin metallic coating are thought to be used as a sensing platform for cell detection. Especially our studies are focused on the detection of circulating tumor cells which are detached from a primary tumor and travel through lymphatic system or bloodstream and indicate the presence of tumor. By modifying these surfaces with certain molecules or biomolecules, biomarkers of specific tumor cells can be targeted. One of our interest is on developing folic acid coated nanoporous alumina-based SERS substrate and target folate receptors which are found in folate receptor-positive circulating tumor cells like metastatic breast, colon and prostate cancer cells.

Further studies are carried out to investigate effects of other mold topographies which can be obtained by changing anodization conditions and use these AAMs as molds. After obtaining polymeric substrates with different topographies, the effect of topography and silver reduction times on SERS signal intensities could be examined. Also studies for fabricating nanostructured biopolymer surfaces from AAM molds are proceeding. With the help of amine groups, reducing metallic ions without the need of polydopamine coating can be achieved. Recently our group focused on fabricating gelatine and chitosan nanopillared surfaces on large surface areas and reduce silver ions on these surfaces without the need of polydopamine coating. These surfaces are intended for the use of the fabricated substrated in this study as reproducible and robust platforms for sensing important cardiac biomarker molecules including myoglobin and troponin-T.



REFERENCES

- [1] **Klabunde, K.J. and Richards, R. eds.**, *Nanoscale materials in chemistry*: Vol. 1035. (Pg.2), New York: Wiley-Interscience. (2001).
- [2] **Martin, C.R.**, (1994). Nanomaterials: a membrane-based synthetic approach, *Science*, pp.1961-1966.
- [3] **Kalantar-zadeh, K. and Fry, B.**, (2007). *Nanotechnology-enabled sensors*. Springer Science & Business Media.
- [4] **Duncan, R. and Gaspar, R.**, (2011). Nanomedicine (s) under the microscope, *Molecular pharmaceuticals*, 8(6), pp.2101-2141.
- [5] **Lee, W. and Park, S.J.**, (2014). Porous anodic aluminum oxide: anodization and templated synthesis of functional nanostructures, *Chemical reviews*, 114(15), pp.7487-7556.
- [6] **O'sullivan, J.P. and Wood, G.C.**, (1970) The morphology and mechanism of formation of porous anodic films on aluminium. In *Proceedings of the Royal Society of London A: mathematical, physical and engineering sciences* (Vol. 317, No. 1531, pp. 511-543). The Royal Society. July.
- [7] **Li, A.P., Müller, F., Birner, A., Nielsch, K. and Gösele, U.**, (1998). Hexagonal pore arrays with a 50–420 nm interpore distance formed by self-organization in anodic alumina. *Journal of applied physics*, 84(11), pp.6023-6026.
- [8] **Nielsch, K., Choi, J., Schwirn, K., Wehrspohn, R.B. and Gösele, U.**, (2002). Self-ordering regimes of porous alumina: the 10 porosity rule. *Nano letters*, 2(7), pp.677-680.
- [9] **Furneaux, R.C., Rigby, W.R. and Davidson, A.P.**, (1989). The formation of controlled-porosity membranes from anodically oxidized aluminium. *Nature*, 337(6203), pp.147-149.
- [10] **Belwalkar, A.A., Huang, Z. and Geertruyden, W.V.**, (2006). Experimental Study Of Nanoporous Ceramic Tube In Potential Application In Hemodialysis. *Asaio Journal*, 52(2), p.75A.
- [11] **Masuda, H. and Fukuda, K.**, (1995). Ordered metal nanohole arrays made by a two-step replication of honeycomb structures of anodic alumina. *science*, 268(5216), p.1466.
- [12] **Shilyaeva, Y.I., Bardushkin, V.V., Gavrilov, S.A., Silibin, M.V., Yakovlev, V.B., Borgardt, N.I., Volkov, R.L., Smirnov, D.I. and Zheludkevich, M.L.**, (2014). Melting temperature of metal polycrystalline nanowires electrochemically deposited into the pores of anodic aluminium oxide. *Physical Chemistry Chemical Physics*, 16(36), pp.19394-19401.
- [13] **Popat, K.C., Swan, E.E.L., Mukhatyar, V., Chatvanichkul, K.I., Mor, G.K., Grimes, C.A. and Desai, T.A.**, (2005). Influence of nanoporous alumina membranes on long-term osteoblast

- response. *Biomaterials*, 26(22), pp.4516-4522.
- [14] **Jani, A.M.M., Losic, D. and Voelcker, N.H.**, (2013). Nanoporous anodic aluminium oxide: advances in surface engineering and emerging applications. *Progress in Materials Science*, 58(5), pp.636-704.
- [15] **Santos, A., Kumeria, T. and Losic, D.**, (2013). Nanoporous anodic aluminum oxide for chemical sensing and biosensors. *TrAC Trends in Analytical Chemistry*, 44, pp.25-38.
- [16] **Kneipp, K., Wang, Y., Kneipp, H., Perelman, L.T., Itzkan, I., Dasari, R.R. and Feld, M.S.**, (1997). Single molecule detection using surface-enhanced Raman scattering (SERS). *Physical review letters*, 78(9), p.1667.
- [17] **Li, J.F., Huang, Y.F., Ding, Y., Yang, Z.L., Li, S.B., Zhou, X.S., Fan, F.R., Zhang, W., Zhou, Z.Y., Ren, B. and Wang, Z.L.**, (2010). Shell-isolated nanoparticle-enhanced Raman spectroscopy. *nature*, 464(7287), pp.392-395.
- [18] **Talley, C.E., Jusinski, L., Hollars, C.W., Lane, S.M. and Huser, T.**, (2004). Intracellular pH sensors based on surface-enhanced Raman scattering. *Analytical chemistry*, 76(23), pp.7064-7068.
- [19] **Barhoumi, A. and Halas, N.J.**, (2010). Label-free detection of DNA hybridization using surface enhanced Raman spectroscopy. *Journal of the American Chemical Society*, 132(37), pp.12792-12793.
- [20] **Ember, K.J., Hoeve, M.A., McAughtrie, S.L., Bergholt, M.S., Dwyer, B.J., Stevens, M.M., Faulds, K., Forbes, S.J. and Campbell, C.J.**, 2017. Raman spectroscopy and regenerative medicine: a review. *npj Regenerative Medicine*, 2(1), p.12.
- [21] **Tian, Z.Q., Ren, B. and Wu, D.Y.**, (2002). Surface-enhanced Raman scattering: from noble to transition metals and from rough surfaces to ordered nanostructures. *J. Phys. Chem. B* 106 (37), pp 9463–9483
- [22] **Kneipp, K., Wang, Y., Kneipp, H., Perelman, L.T., Itzkan, I., Dasari, R.R. and Feld, M.S.**, (1997). Single molecule detection using surface-enhanced Raman scattering (SERS). *Physical review letters*, 78(9), p.1667.
- [23] **Hao, E. and Schatz, G.C.**, (2004). Electromagnetic fields around silver nanoparticles and dimers. *The Journal of chemical physics*, 120(1), pp.357-366.
- [24] **Nie, S. and Emory, S.R.**, (1997). Probing single molecules and single nanoparticles by surface-enhanced Raman scattering. *science*, 275(5303), pp.1102-1106.
- [25] **Bezares, F.J., Caldwell, J.D., Glembocki, O., Rendell, R.W., Feygelson, M., Ukaegbu, M., Kasica, R., Shirey, L., Bassim, N.D. and Hosten, C.**, (2012.). The role of propagating and localized surface plasmons for SERS enhancement in periodic nanostructures. *Plasmonics*, 7(1), pp.143-150.
- [26] **Kleinman, S.L., Frontiera, R.R., Henry, A.I., Dieringer, J.A. and Van Duyne, R.P.**, (2013). Creating, characterizing, and controlling chemistry with SERS hot spots. *Physical Chemistry Chemical Physics*, 15(1), pp.21-36.

- [27] **Banholzer, M.J., Millstone, J.E., Qin, L. and Mirkin, C.A.,** (2008). Rationally designed nanostructures for surface-enhanced Raman spectroscopy. *Chemical Society Reviews*, 37(5), pp.885-897.
- [28] **Cialla, D., März, A., Böhme, R., Theil, F., Weber, K., Schmitt, M. and Popp, J.,** (2012). Surface-enhanced Raman spectroscopy (SERS): progress and trends. *Analytical and bioanalytical chemistry*, 403(1), pp.27-54.
- [29] **Jackson, J.B. and Halas, N.J.,** (2004). Surface-enhanced Raman scattering on tunable plasmonic nanoparticle substrates. *Proceedings of the National Academy of Sciences*, 101(52), pp.17930-17935.
- [30] **Fan, M., Andrade, G.F. and Brolo, A.G.,** (2011). A review on the fabrication of substrates for surface enhanced Raman spectroscopy and their applications in analytical chemistry. *Analytica chimica acta*, 693(1), pp.7-25.
- [31] **Cölfen, H. and Mann, S.,** (2003). Higher- order organization by mesoscale self- assembly and transformation of hybrid nanostructures. *Angewandte Chemie International Edition*, 42(21), pp.2350-2365.
- [32] **Gomar-Nadal, E., Puigmartí-Luis, J. and Amabilino, D.B.,** (2008). Assembly of functional molecular nanostructures on surfaces. *Chemical Society Reviews*, 37(3), pp.490-504.
- [33] **Cha, H.R., Lee, J., Lee, J.W., Kim, J.M., Lee, J., Gwak, J., Yun, J.H., Kim, Y. and Lee, D.,** (2012). Microfabrication and optical properties of highly ordered silver nanostructures. *Nanoscale research letters*, 7(1), p.292.
- [34] **Zhang, C., Abdijalilov, K. and Grebel, H.,** (2007). Surface enhanced Raman with anodized aluminum oxide films. *The Journal of chemical physics*, 127(4), p.044701.
- [35] **Ko, H. and Tsukruk, V.V.,** (2008). Nanoparticle- decorated nanocanals for surface- enhanced raman scattering. *small*, 4(11), pp.1980-1984.
- [36] **Terekhov, S.N., Mojzes, P., Kachan, S.M., Mukhurov, N.I., Zhvavyi, S.P., Panarin, A.Y., Khodasevich, I.A., Orlovich, V.A., Thorel, A., Grillon, F. and Turpin, P.Y.,** (2011). A comparative study of surface- enhanced Raman scattering from silver- coated anodic aluminum oxide and porous silicon. *Journal of Raman Spectroscopy*, 42(1), pp.12-20.
- [37] **Cui, J., Wu, Y., Wang, Y., Zheng, H., Xu, G. and Zhang, X.,** (2012). A facile and efficient approach for pore-opening detection of anodic aluminum oxide membranes. *Applied Surface Science*, 258(14), pp.5305-5311.
- [38] **Xu, B.B., Zhang, Y.L., Zhang, W.Y., Liu, X.Q., Wang, J.N., Zhang, X.L., Zhang, D.D., Jiang, H.B., Zhang, R. and Sun, H.B.,** (2013). Silver- coated rose petal: green, facile, low- cost and sustainable fabrication of a SERS substrate with unique superhydrophobicity and high efficiency. *Advanced Optical Materials*, 1(1), pp.56-60.
- [39] **Chu, S.Z., Wada, K., Inoue, S., Isogai, M. and Yasumori, A.,** (2005). Fabrication of Ideally Ordered Nanoporous Alumina Films and Integrated Alumina Nanotubule Arrays by High- Field Anodization. *Advanced materials*, 17(17), pp.2115-2119

- [40] **Belwalkar, A., Grasing, E., Van Geertruyden, W., Huang, Z. and Misiolek, W.Z.,** (2008). Effect of processing parameters on pore structure and thickness of anodic aluminum oxide (AAO) tubular membranes. *Journal of membrane science*, 319(1), pp.192-198.
- [41] **Xu, T., Zangari, G. and Metzger, R.M.,** (2002). Periodic holes with 10 nm diameter produced by grazing Ar⁺ milling of the barrier layer in hexagonally ordered nanoporous alumina. *Nano Letters*, 2(1), pp.37-41.
- [42] **Altuntas, S., Buyukserin, F., Haider, A., Altinok, B., Biyikli, N. and Aslim, B.,** (2016). Protein-releasing conductive anodized alumina membranes for nerve-interface materials. *Materials Science and Engineering: C*, 67, pp.590-598.
- [43] **Pashchanka, M. and Schneider, J.J.,** (2011). Origin of self-organisation in porous anodic alumina films derived from analogy with Rayleigh-Bénard convection cells. *Journal of Materials Chemistry*, 21(46), pp.18761-18767.
- [44] **Lang, X., Qiu, T., Zhang, W., Yin, Y. and Chu, P.K.,** (2011). Tunable silver nanocap superlattice arrays for surface-enhanced Raman scattering. *The Journal of Physical Chemistry C*, 115(49), pp.24328-24333.
- [45] **Wang, J., Huang, L., Zhai, L., Yuan, L., Zhao, L., Zhang, W., Shan, D., Hao, A., Feng, X. and Zhu, J.,** (2012). Hot spots engineering in hierarchical silver nanocap array for surface-enhanced Raman scattering. *Applied Surface Science*, 261, pp.605-609.
- [46] **Nicolai, S.H. and Rubim, J.C.,** (1994). Effect of molecular oxygen on the surface-enhanced Raman intensity of adsorbed molecules on silver, copper and gold electrodes. *Vibrational spectroscopy*, 7(2), pp.175-183.
- [47] **Dick, L.A., McFarland, A.D., Haynes, C.L. and Van Duyne, R.P.,** (2002). Metal film over nanosphere (MFON) electrodes for surface enhanced Raman spectroscopy (SERS): Improvements in surface nanostructure stability and suppression of irreversible loss. *The Journal of Physical Chemistry B*, 106(4), pp.853-860.
- [48] **Altuntas, S. and Buyukserin, F.,** (2014). Fabrication and characterization of conductive anodic aluminum oxide substrates. *Applied Surface Science*, 318, pp.290-296.
- [49] **Akin, M.S., Yilmaz, M., Babur, E., Ozdemir, B., Erdogan, H., Tamer, U. and Demirel, G.,** (2014). Large area uniform deposition of silver nanoparticles through bio-inspired polydopamine coating on silicon nanowire arrays for practical SERS applications. *Journal of Materials Chemistry B*, 2(30), pp.4894-4900.
- [50] **Dandapat, A., Lee, T.K., Zhang, Y., Kwak, S.K., Cho, E.C. and Kim, D.H.,** (2015). Attomolar level detection of Raman molecules with hierarchical silver nanostructures including tiny nanoparticles between nanosized gaps generated in silver petals. *ACS applied materials & interfaces*, 7(27), pp.14793-14800.
- [51] **Liu, X., Shao, Y., Tang, Y. and Yao, K.F.,** (2014). Highly uniform and reproducible surface enhanced Raman scattering on air-stable

- metallic glassy nanowire array. *Scientific reports*, 4.
- [52] Lee, C., Robertson, C.S., Nguyen, A.H., Kahraman, M. and Wachsmann-Hogiu, S., (2015). Thickness of a metallic film, in addition to its roughness, plays a significant role in SERS activity. *Scientific reports*, 5, p.11644.
- [53] Fu, C.Y., Kho, K.W., Dinish, U.S., Koh, Z.Y. and Malini, O., (2012). Enhancement in SERS intensity with hierarchical nanostructures by bimetallic deposition approach. *Journal of Raman Spectroscopy*, 43(8), pp.977-985.
- [54] Bonancêa, C.E., do Nascimento, G.M., De Souza, M.L., Temperini, M.L. and Corio, P., (2006). Substrate development for surface-enhanced Raman study of photocatalytic degradation processes: Congo red over silver modified titanium dioxide films. *Applied Catalysis B: Environmental*, 69(1), pp.34-42.
- [55] Liang, H., Li, Z., Wang, W., Wu, Y. and Xu, H., (2009). Highly Surface-roughened "Flower-like" Silver Nanoparticles for Extremely Sensitive Substrates of Surface-enhanced Raman Scattering. *Advanced Materials*, 21(45), pp.4614-4618.
- [56] García-Vidal, F.J. and Pendry, J.B., (1996). Collective theory for surface enhanced Raman scattering. *Physical Review Letters*, 77(6), p.1163.
- [57] Lin, X.M., Cui, Y., Xu, Y.H., Ren, B. and Tian, Z.Q., (2009). Surface-enhanced Raman spectroscopy: substrate-related issues. *Analytical and bioanalytical chemistry*, 394(7), pp.1729-1745.
- [58] Porter, M.D., Lipert, R.J., Siperko, L.M., Wang, G. and Narayanan, R., (2008). SERS as a bioassay platform: fundamentals, design, and applications. *Chemical Society Reviews*, 37(5), pp.1001-1011.
- [59] Chen, J., Qin, G., Wang, J., Yu, J., Shen, B., Li, S., Ren, Y., Zuo, L., Shen, W. and Das, B., (2013). One-step fabrication of sub-10-nm plasmonic nanogaps for reliable SERS sensing of microorganisms. *Biosensors and Bioelectronics*, 44, pp.191-197.
- [60] El-Said, W.A., Fouad, D.M. and El-Safty, S.A., (2016). Ultrasensitive label-free detection of cardiac biomarker myoglobin based on surface enhanced Raman spectroscopy. *Sensors and Actuators B: Chemical*, 228, pp.401-409.
- [61] Ji, N., Ruan, W., Wang, C., Lu, Z. and Zhao, B., (2009). Fabrication of silver decorated anodic aluminum oxide substrate and its optical properties on surface-enhanced Raman scattering and thin film interference. *Langmuir*, 25(19), pp.11869-11873.
- [62] Daglar, B., Demirel, G.B., Khudiyev, T., Dogan, T., Tobail, O., Altuntas, S., Buyukserin, F. and Bayindir, M., (2014). Anemone-like nanostructures for non-lithographic, reproducible, large-area, and ultra-sensitive SERS substrates. *Nanoscale*, 6(21), pp.12710-12717.
- [63] Lee, H., Dellatore, S.M., Miller, W.M. and Messersmith, P.B., (2007). Mussel-inspired surface chemistry for multifunctional coatings. *science*, 318(5849), pp.426-430.
- [64] Yilmaz, M., Bakirci, G., Erdogan, H., Tamer, U. and Demirel, G., (2016). The fabrication of plasmonic nanoparticle-containing multilayer films via a bio-inspired polydopamine coating. *RSC*

Advances, 6(15), pp.12638-12641.

- [65] **Altuntas, S.** (2013) Nanoporlu Anotlanmış Alüminyum Oksit Membranların İlaç Taşıma ve Sinir-Doku Mühendisliği Uygulamaları için Kullanımının Araştırılması (Yüksek Lisans Tezi). Adres: <http://etu.edu.tr>
- [66] **Chen, J., Qin, G., Wang, J., Yu, J., Shen, B., Li, S., Ren, Y., Zuo, L., Shen, W. and Das, B.,** (2013). One-step fabrication of sub-10-nm Plasmonic nanogaps for reliable SERS sensing of microorganisms. *Biosensors and Bioelectronics*, 44, pp.191-197.



BIOGRAPHICAL SKETCH

Name-Surname : Merve ÇELİK
Nationality : TC
Date and Place of Birth : 27.05.1993 Ankara
E-mail : mervcellik@gmail.com

EDUCATION:

- **Bachelor Degree** : 2015, Başkent University, Biomedical Engineering
- **Master Degree** : 2017, TOBB University of Economics and Technology, Biomedical Engineering

JOB EXPERIENCE:

Year	Place	Duty
2013	GATA Hospital	Internship
2014	PENTA Tıbbi Cihazlar ve Bilişim Sistemleri San. ve Tic. A.Ş	Internship
2014	Carl Zeiss Meditec Medikal Çözümler Tic. ve San. A.Ş	Marketing Assist.
2016	TOBB University of Economics and Technology	Scholarship Student

FOREIGN LANGUAGE:

English (Advanced)
Turkish (Advanced)
German (Intermediate)

PUBLICATIONS:

- **Celik, M.**, Altuntas, S. and Buyukserin, F., 2017. Fabrication of nanocrater-decorated anodic aluminum oxide membranes as substrates for reproducibly enhanced SERS signals. *Sensors and Actuators B: Chemical*.
- **Celik, M.**, Altuntas, S. and Buyukserin, F., 2017. Investigation of the Use of Nanocrater-decorated Anodic Aluminum Oxide Membranes as Substrates for Reproducibly Enhanced SERS Signals, International Conference on Nanomedicine and Nanobiotechnology, September 25-27, Barcelona Spain.
- **Celik, M.**, Altuntas, S. and Buyukserin, F., 2017, Investigation of the Use of Anodic Aluminum Oxide Membranes as SERS Substrates and Detection of Myoglobin, International Conference on Medical and Biological Engineering, March 16-18, Sarajevo, Bosnia and Herzegovina .
- **Celik, M.**, Altuntas, S. and Buyukserin, F., 2016, Investigation of the use of Periodic Nanobump Surfaces For Detecting Myoglobin Protein, 3rd International Conference on Biosensors, October 5-7, Ankara, Turkey.
- **Celik, M.**, Altuntas, S. and Buyukserin, F., 2016, Investigation of the use of peiodic nanobump structures for detecting Alzheimers disease, XXV International Material Research Congress, August 14-19, Cancun, Mexico.